

Mobilization of geochemical elements in the active layer of permafrost to surface water in Russian Arctic

Xiaowen Ji¹, Xianchuan Xie², Evgeny Abakumov³, and Vyacheslav Polyakov⁴

¹School of Environment and Sustainability

²Nanjing University

³Saint-Petersburg State University

⁴Arctic and Antarctic Research Institute

November 24, 2022

Abstract

The predicted increasing ground temperatures in the Arctic results in the deepening of the active layer and intensification of geochemical processes, which could affect the geochemical composition of surface waters. Determining the responses of the riparian soil systems to surrounding hydrological flows under changing climate conditions is important for understanding the seasonal changes in hydrological processes. Therefore, in this study, one soil core from the study area polygon rim (close to the Taz River, TA) and two soil cores from the riverain terrace (close to the Syoyakha River, SY and Murtyyakha River, MU) in Russian Western Siberia and their supra-permafrost water, adjacent stream flows and river water were sampled for analysis of geochemical elements. The results showed that most elements above their respective detection limits (Mn, Sr, Fe, Mg, Cr, Co, V, Pb, Al and Ca) started to accumulate in the downwards gleyed layer during September–October in response to the deepest thaw in the active layer. This study focused on the highly mobile elements, i.e., Mn, Ca, Mg, Al and Ti, in the deepest layer; and found the transport of organic matter in the upper layer carried these elements to both surface water ponds/flows and supra-permafrost water, and further, to the rivers. The best linear correlation for both stream flows and river water were Mn, which may be a proxy for predicting the processes occurring within the active layer during the annual summer-autumn thaw. Finally, landscapes with different ice contents may experience changes in the elements transported to surface waters.

Hosted file

essoar.10502798.1.docx available at <https://authorea.com/users/544758/articles/603025-mobilization-of-geochemical-elements-in-the-active-layer-of-permafrost-to-surface-water-in-russian-arctic>

1

1 **Mobilization of geochemical elements in the active layer of**
2 **permafrost to surface water in Russian Arctic**

3

4 **Xiaowen Ji^{a,b,c}, Evgeny Abakumov^b, Vyacheslav Polyakov^{b,d,e}, Xianchuan Xie^{a*}**

5

6 ^a *State Key Laboratory of Pollution Control and Resource Reuse, School of the Environment,*
7 *Nanjing University, Nanjing, 210093, P. R. China*

8 ^b *Department of Applied Ecology, Saint Petersburg State University, Saint Petersburg,*
9 *199178, Russian Federation*

10 ^c *School of Environment and Sustainability, University of Saskatchewan, Saskatoon SK, S7N*
11 *5B3, Canada*

12 ^d *Arctic and Antarctic Research Institute, Saint Petersburg, 199397, Russian Federation*

13 ^e *Department of Soil Science and Agrochemistry, Saint-Petersburg State Agrarian University,*
14 *Pushkin, Saint Petersburg, 19660, Russian Federation*

15

16 * Corresponding author's e-mail: xchxie@nju.edu.com

2

3

17 **Abstract**

18 The predicted increasing ground temperatures in the Arctic results in the deepening of the active
19 layer and intensification of geochemical processes, which could affect the geochemical
20 composition of surface waters. Determining the responses of the riparian soil systems to
21 surrounding hydrological flows under changing climate conditions is important for understanding
22 the seasonal changes in hydrological processes. Therefore, in this study, one soil core from the
23 study area polygon rim (close to the Taz River, TA) and two soil cores from the riverain terrace
24 (close to the Syoyakha River, SY and Murtyyakha River, MU) in Russian Western Siberia and
25 their supra-permafrost water, adjacent stream flows and river water were sampled for analysis of
26 geochemical elements. The results showed that most elements above their respective detection
27 limits (Mn, Sr, Fe, Mg, Cr, Co, V, Pb, Al and Ca) started to accumulate in the downwards gleyed
28 layer during September–October in response to the deepest thaw in the active layer. This study
29 focused on the highly mobile elements, i.e., Mn, Ca, Mg, Al and Ti, in the deepest layer; and
30 found that the transport of organic matter in the upper layer carried these elements to both surface
31 water ponds/flows and supra-permafrost water, and further, to the rivers. The best linear
32 correlation for both stream flows and river water were Mn, which may be a proxy for predicting
33 the processes occurring within the active layer during the annual summer-autumn thaw. Finally,
34 landscapes with different ice contents may experience changes in the elements transported to
35 surface waters.

36

37 **Keywords:** Geochemical elements, Arctic, Permafrost-affected soils, active layer, surface water,
38 seasonal thawing

39

40 **1. Introduction**

41 The increasing atmospheric temperatures in the Arctic have led to permafrost thawing and
42 vertical downward migration of the active layer into formerly frozen ground, during the thawing
43 season (Christiansen et al. 2010, Connon et al. 2018, Jorgenson et al. 2010, Romanovsky et al.
44 2010, Smith et al. 2010). The active layer responds to the changing climatic conditions by
45 increasing its depth, thus accelerating chemical weathering (Colombo et al. 2019, Keller et al.
46 2007, 2010) and potentially releasing geochemical components and organic carbon from the soil
47 to adjacent aquatic landscapes (Barker et al. 2014, Grosse et al. 2016, Johnson et al. 2013,
48 Johnston et al. 2014, Loiko et al. 2017, Raudina et al. 2018, Schuur et al. 2015). This would
49 increase the movement of carbon dioxide (CO₂) from the soil to aquatic reservoirs such as rivers
50 and lakes (Elder et al. 2019, Natali et al. 2015, Polishchuk et al. 2018, Wild et al. 2019); this
51 occurs through the transport of solute and water along surface streams and the permafrost table,
52 which is as known as “supra-permafrost flow”. Supra-permafrost water is found in the shallow
53 subsurface of the active layer, where it is typically situated at the boundary between the frozen and
54 thawed fractions of the soil profile (Cederstrom et al. 1953). Owing to the absence of groundwater
55 discharge in the permafrost-affected region, solutes being transported to lakes or rivers from
56 adjacent soils originate primarily from supra-permafrost water.

57 Permafrost degradation has been associated with an increased contribution of groundwater to
58 stream via surface flows or supra-permafrost water in Canadian Arctic rivers (Walvoord and
59 Striegl 2007). Ice wedge degradation has also been proven to be related to the water balance of
60 lowland across the Arctic landscapes, and to increase streamflow (Liljedahl et al. 2016). Several
61 studies have observed substantial increments in discharges from the major Eurasian Arctic rivers
62 due to the warming climate (Brown et al. 2019, Feng et al. 2019, Lammers et al. 2001, Yang et
63 al. 2002, Zheng et al. 2019). Raudina et al. (2018) observed a northward shift of the permafrost
64 boundary under climate change scenarios, and that the concentrations of dissolved organic carbon
65 (DOC), major and trace elements, and greenhouse gases are expected to decrease in the supra-
66 permafrost waters at the border between the thawed and frozen parts from peat soils in the western
67 Siberia lowland. Loiko et al. (2017) hypothesized that the direct mobilization of soil waters to

68 hydrological networks and the transformation of autochthonous processes were controlled by
69 physical factors in different landscapes. Overall, there appears to be considerable variability and
70 uncertainty regarding how discharges of DOC, elements, and greenhouse gases in supra-
71 permafrost waters/surface flows respond to permafrost thaw and are released to surface water
72 ponds and rivers.

73 Several studies concerning the biogeochemical cycles of carbon and related metals focused
74 on both the aquatic and the terrestrial parts of the continental permafrost-bearing ecosystem (Guo
75 et al. 2007, McClelland et al. 2007, Olefeldt and Roulet 2012, Pokrovsky et al. 2011). More
76 recently, the biogeochemistry of soil porewater and supra-permafrost water in mineral and
77 organic/peat parts of soil profiles in the permafrost areas have been studied (Barker et al. 2014,
78 Jessen et al. 2014, Lamhonwah et al. 2017, Loiko et al. 2017, Raudina et al. 2018, Street et al.
79 2016). The previous studies concluded that the export fluxes of DOC, greenhouse gases, and trace
80 metals from the active layer of permafrost to the surrounding hydrological landscapes are
81 determined by the amount of water passing through the active layer till the border of the frozen
82 permafrost, before being drained to a lake or river (Pokrovsky et al. 2016a, Pokrovsky et al.
83 2016b, Raudina et al. 2018). Barker et al. (2014) reported that the concentrations of metals in
84 surface water were related to the increasing active layer thickness/degrading permafrost during
85 late fall and early winter. These results revealed that the dynamics of trace metal concentrations in
86 the transitions from Arctic soils to surface water corresponded to top-down freezing processes in
87 the active layer. However, there is a lack of information connecting geochemical tracers in both
88 the underlying supra-permafrost flow and the upper soil layer to explain the transport of
89 geochemical compositions to surrounding hydrological networks and can be used as a proxy for
90 the seasonal active layer dynamics.

91 Therefore, this study aims to provide this knowledge by analyzing supra-permafrost water, soil
92 pore water, surrounding small water ponds/flows, and eventually, river surface water from three
93 typical soils close to rivers from continuous permafrost regions within the Yamal and Gydan
94 peninsulas, West Siberian Arctic. Tundra lakes and river floodplains are abundant in the Yamal and
95 Gydan peninsulas; lakes cover, on average, 10% of the Yamal peninsula, occupying 20% of the
96 floodplains of large rivers (Dvornikov et al. 2019). Approximately 90% of all lakes in the study

97 region are small (<1 km²) water bodies. To analyze the effluxes of permafrost soils from relatively
98 homogeneous landscapes, the sampling sites were set up next to the largest rivers flowing to the
99 Kara sea, such as the Syoyakha, Murtyyakha, and Taz Rivers. Our main working hypotheses are as
100 follows: (i) Based on the response of riverine DOC and element concentrations to increasing
101 active layer thickness reaches the highest contents during late autumn, when the active layer
102 reaches its greatest depth in a year. Besides, when the components' concentrations in the base flow
103 increases, with the yearly maximum values being observed in the Siberian rivers (Yang et al.
104 2002). Therefore, the dominant contributor of DOC and trace elements to river waters during this
105 time of the year is expected to be supra-permafrost water and base flow to the rivers. (ii) When
106 mineral weathering processes continue in the deeper soil column during late autumn and early
107 winter, shallow subsurface soil can also store major mobilized components, such as DOC, in late
108 autumn during freezing; these components bind with elements and can contribute to spring thaw in
109 the next year. Formerly mobilized components stored in the shallow subsurface during spring
110 snowmelt can be potentially enhanced to supra-permafrost waters and further to surrounding
111 surface waters. Therefore, with an increasing thawed depth of permafrost and the potentially
112 enhanced mineral weathering fluxes into supra-permafrost waters, biogeochemical fluxes from
113 surrounding surface waters may experience a change during spring and autumn. (iii) As the DOC
114 and elements are controlled by the redox environment of riparian soils, they cannot be consumed
115 by the surrounding biota or depleted by abiotic reaction, and thence persist in supra-permafrost
116 water; they may be transported to the surrounding hydrological network.

117 The specific objectives of this study were (1) to assess the mobility of releasing geochemical
118 elements from upper soil layer water and supra-permafrost water to surrounding water bodies; (2)
119 to examine whether the concentrations of geochemical elements in the surface water (connected
120 streams and received river) can explain the active layer dynamics of permafrost riparian soils in
121 different permafrost-affected landscapes.

122

123 2. Studying site and methods

124 2.1 Geographical setting

125 The study area was located in the Northwest area of the Yamal-Nets Autonomous Region,
126 across 66° N, with continuous permafrost (**Figure 1A**). Sampling sites were located close to
127 the lowlands of the Syoyakha, Murtyyakha, and Taz rivers. The Syoyakha and Murtyyakha
128 Rivers are situated in the Yamal Peninsula on the Western Siberian plain (Golovatin et al.
129 2011). These geographical features of this region are strongly divided between river valleys,
130 lake hollows, and streams (Golovatin et al. 2011). Cryogenic soils in this part of the Yamal
131 Peninsula were formed due to the high ice content of Holocene alluvial sediments (Sidorchuk
132 and Grigorev 1998) and aeolian materials (Alekseev and Abakumov 2018). This part of the
133 lowland comprises very flat watersheds of the Syoyakha and Murtyyakha Rivers and is
134 covered with frozen bogs and palsa. The Syoyakha is one of the largest rivers of the Yamal
135 Peninsula (Bespalaya et al. 2018); its watercourse is 165 km long and its watershed covers an
136 area of 4,400 km² (Bespalaya et al. 2018). The Murtyyakha River has roughly 580
137 watercourses and numerous lakes in its basin, which contains 70 rivers more than 10 km long.
138 The Murtyyakha River flows into the Syoyakha River and then enters Kara Sea. Syngenetic
139 permafrost close to these two rivers contains massive Holocene ice deposits (Vasil'chuk et al.
140 2016). The 1,401 km long Taz River is located in the Gydan Peninsula and drains a basin of
141 150,000 km²; it flows into the Taz Estuary and ends in the Gulf of Ob. Soils along with the
142 river included alluvial stratified parent deposits from an earlier stage of the Holocene
143 (Tarnocai 2009).

144 We investigated the three poorly drained riparian soils with upper organic layers and a
145 downward mineral profile adjacent to each river (**Figure 1A**). The soil close to the Taz River
146 site (TA) was located at the top of the polygon rim, where the landscape is polygonal tundra,
147 and the center of polygon was wet-depressed and an accumulation of organic matter poorly
148 degraded by anaerobic conditions; the surrounding elevated polygon rim showed the evidence

149 of cryoturbation in most horizons in the active layer (**Figure 1B**). The soil profile was gleyed
150 with frost heaving of the clay stratum. The surrounding vegetation consists predominantly of
151 wet acidic tussock sedge, grass, and sphagnum moss. Soils sampled nearby at the Syoyakha
152 (SY) and Murtyyakha (MU) Rivers were both situated from the floodplain. The SY site
153 consisted of moist acidic moss, lichen, and sedges, and MU site consisted of lingonberry,
154 willow, moss, and sedge. Both soil profiles had shallow active layers that were strongly
155 gleyed and under reducing conditions, while the deeper layers at MU showed obvious signs of
156 cryoturbation (**Figure 1C and D**). The formation of the SY and MU stratified soils may have
157 resulted from the constant changes in the river water levels. All three soil profiles for TA, SY,
158 and MU have been depicted as relatively light chroma color with oxidation of iron minerals
159 and dominated by mineral substrates with allochthonous organic matter or autochthonous
160 peat.

161 **2.2 Soil core and supra-permafrost water collection and analysis**

162 Three soil cores were extracted up to the permafrost table using a portable Snow-Ice
163 Permafrost-Research-Establishment (SIPRE) auger set consisting of a coring auger and an
164 engine from Jon's Machine Shop, Fairbanks, Alaska, USA. The location of each soil core was
165 directly adjacent to the borehole into which a string thermometer was inserted (**Figure 1A**).
166 The thermometers, which were put in cases filled with grease as an inert material, were placed
167 roughly 10 cm from permafrost table for 24 h in July 2016 in order to reach thermal
168 equilibrium with surrounding soil material. The thermometers were connected to a data logger
169 for recording hourly temperatures in degrees Celsius (Modular GM10, Yokogawa Electric
170 Corporation, Tokyo, Japan), powered by a battery with a three-year life and attached to a
171 stainless-steel stake inserted into the soil cores. The excavated local soils were moved back to
172 the soil cores. The cores were collected in May 2016, sealed with Polyethylene covers,
173 transported at a stable temperature of -4 °C to freeze the soils, and stored in a refrigerator at
174 the same temperature prior to analysis. We believe the cores can partially reflect the deepest
175 active layer during a year, with approximately 65 cm for Mu, 46 cm for Sy, and 90 cm for Ta

176 shown by the thawing materials. The soil pits were excavated in July 2017 adjacent to the
177 coring location (**Figure 1**), and site restoration procedures followed the standard protocols for
178 permafrost-affected soils (Ping et al. 2013). Excavating soil pits may provide an insight into
179 the vertical depth between the active layer and permafrost that contain external flows to
180 rivers. Each 35 × 35 cm soil pit was excavated with a shovel and hatchet until reaching frozen
181 materials and the genetic horizon and name of each soil were identified using the World
182 Reference Base for Soil Resources WRB (2015) classification system. The stagnic condition
183 of soils meant that we had to use 2,2'-Dipyridyl to spray soils for 30 s to test for reducing
184 conditions, as per the tests previously conducted on gleyed soils (Ping et al. 1998).

185 The frozen soil core was cut into 5 cm sections with a diamond wire saw (LKH-8, Kanghua
186 Company, Guilin, China), with a cutting section of diamond-impregnated wire mounted on
187 idler pulleys, in a cold room in the laboratory of Arctic Logistics Center, Salekhard, Yamal-
188 Nenets Autonomous Region, Russia. The cut sections of each soil core were then placed in
189 tightly sealed plastic bags (9.5 cm x 18 cm, Bag Whirlpak Clear 7oz, Nasco, FL, US) and
190 kept at room temperature (approximately 23 °C) to thaw for 12 h. Completely thawed soils
191 were used to collect soil porewater with an SPS 200 lysimeter soil solution sampler (SDEC,
192 Reignac-sur-Indre, France). The collected water was filtered through a 0.45 µm
193 polypropylene filter, decanted to glass test tubes, and acidified with 0.5(wt) % ultrapure nitric
194 acid (HNO₃, CAS: 7697-37-2 Fisher Scientific, Hampton, USA) before processing through
195 inductively coupled plasma-tandem mass spectrometry (8800 ICP-MS/MS, Agilent, Santa
196 Clara CA, USA). To remove the spectral interferences of ions through ion/neutral reactions,
197 the collision reaction cells (CRCs) mode in the ICP-MS was operated using He or NH₃ as the
198 inert collision gas, following the protocol developed by McCurdy and Woods (2004). The
199 elements V, Cr, Mn, Fe, Co, Ni, Cu, Zn, and As were analyzed in CRCs mode with He gas to
200 remove unidentified polyatomic particles arising from the variables Cl⁻, S⁻, and C⁻. Ti was
201 analyzed in CRCs mode with NH₃ to remove interference from S-based polyatomic ions. The
202 elements Sr, K, Ca, Mg, Al, Ba, Be, B, Cd, Pb, Au, Mo, P, Sc, Ag, Tl, Sn, and rare earth

203 elements (REEs) were analyzed using normal (non-CRCs) mode.

204 Four calibration standards (1×10^{-2} , 1×10^{-1} , 1×10^1 , $1 \times 10^2 \mu\text{g L}^{-1}$) were prepared by diluting
205 $1 \times 10^3 \mu\text{g L}^{-1}$ stock standard solution for each element and mixed REEs (TraceCERT®)
206 purchased from Sigma-Aldrich, St. Louis MO USA. The 2% (w/w) ultrapure HNO_3 was taken
207 as the blank. Calibration was performed before every analytical test with a good calibration
208 curve ($R^2 \approx 0.999$), and three blanks and check standards were run before every ten samples.
209 The analytical uncertainty for each sample was determined by the analysis of triplicate within
210 an error of $\pm 3\%$. The detection limits for all elements were set at the level of $1 \mu\text{g L}^{-1}$. To
211 correct the magnitude of the signal suppression or enhancement, a standard mixture solution
212 of Bi, Ge, In, Li, Sc, Tb, and Y ($10 \mu\text{g /mL}$) prepared in 2% ultrapure HNO_3 was used as the
213 internal standard added in all standards, blanks, and samples.

214 Then, each soil core section was transported to the Applied Ecological Laboratory, Saint
215 Petersburg State University. They were dried in a vacuum drying oven for 16 h, homogenized
216 by grinding using a roller mill, processed through a 2-mm sieve, and finally, soils were
217 pressed into a powder pellet with a vertical hydraulic jack. Each pellet was analyzed through
218 scanning electron microscopy with energy dispersive X-ray spectroscopy (SEM-EDX) (JSM-
219 6390 LA, EX2300, JEOL, Tokyo, Japan). EDX revealed the characteristic peak for each
220 metal in each sample with atomic-level precision, which can directly transfer the
221 concentration in terms of mg kg^{-1} . The soil certified reference material CRM027 and
222 SQC001-30G (Sigma-Aldrich, St. Louis, USA) for trace metals were used for calibration.
223 Samples and the reference material were analyzed in triplicate, and the detection limits were
224 determined based on the minimum value of the reference material.

225 The location of stagnant supra-permafrost waters was collected adjacent to the previous
226 soil cores in September 2016. To prevent the contamination of water samples due to the
227 previous methods of collecting supra-permafrost waters with soil pit excavation, an alloy
228 probe rod was first inserted into the soil to confirm approximately the same depth of the
229 active layer–permafrost boundary as the previous soil core. A direct push device (SP16

230 Groundwater Sampler, Geoprobe Systems®, Salina KS USA) comprising a polyvinyl
231 chloride screen was driven to the permafrost table within a sealed steel sheath. Then, the
232 water samples were pumped through the tube to the surface and stored in 25-mL PVC serum
233 bottles by oscillating the tubing up and down.

234 For the lower floodplain (SY and MU), water samples were collected after pumping the
235 tube for 15–20 min to flush water with permafrost materials. The time required for pumping
236 water in TA was relatively longer than that for the other sites, by approximately 30 min, with
237 less volume of inflowing water because of the higher depth of polygon rim. For all sites, the
238 first portion of water containing permafrost materials was discarded, and the clearer water
239 with fewer impurities was collected. Unfiltered water Samples in the serum bottles were
240 treated with 0.2 mL of mercuric chloride (HgCl_2 , Sigma-Aldrich) and capped without air
241 bubbles or headspace using butyl rubber stoppers pierced by a needle attached to a 3-mL
242 syringe that allows air and water escape from the bottle when the stopper is inserted. With the
243 bottle inverted, 10 ml of methane-free helium (Sigma-AldricFh) was added, meanwhile 10 ml
244 of water was removed through needle displacement and the syringe. Then, another 10 ml of
245 methane-free helium was added to the headspace without removing water, and water and
246 headspace were equilibrated in the bottle by shaking for 2 min. The triplicates of subsample
247 headspace gas (into the syringe) were analyzed for CH_4 and CO_2 by gas chromatography (GC-
248 456, Bruker, Billerica MA, USA), with flame-ionization detection (FID) and electron capture
249 detection (ECD), respectively. After each set of ten samples, the detectors were calibrated
250 based on Air Liquide ($\text{CO}_2 = 246.6 \mu\text{mole/mole}$, $\text{CH}_4 = 302.3 \mu\text{mole/mole}$). The results of
251 triplicate injection showed a repetition rate within $\pm 2\%$. The gas solubility of CH_4 and CO_2
252 (Kastanidis et al. 2018) were taken by calculating the total concentration of CH_4 and CO_2 in
253 the vials and then converting to $\mu\text{mol/L}$ of the initial samples. All analysis procedures for
254 analyzing CH_4 and CO_2 were carried out in the Center for Chemical Analysis and Materials
255 Research of St. Petersburg State University. The water temperature, dissolved oxygen, pH,
256 and specific conductivity were field measured with a portable multiparameter meter (Orion

257 Star™ A329, ThermoFischer Scientific, Waltham MA, USA). Stagnant supra-permafrost
258 waters in this study were oxygenated with an average O₂ saturation in samples ranging from
259 10.2 to 82.3% with an uncertainty of 3-4%, which is very close to the previous reports in
260 Western Siberian lowlands (Loiko et al. 2017, Raudina et al. 2018). No significant difference
261 was observed in the O₂ concentrations from water samples in each soil site. The average
262 temperature of supra-permafrost waters did not vary significantly as 12.3±1.8 °C for SY,
263 13.4±1.6 °C for MU, and 15.6±2.0 °C for TA. The dissolved organic carbon (DOC)
264 concentrations were analyzed by a TOC-L TOC Analyzer (Shimadzu Kyoto, Japan) with an
265 uncertainty of 5% and a detection limit of 4 µg/L.

266 **2.3 Surface water collection and analysis**

267 All surface water samples were collected in September 2016. All sampling sites were
268 adjacent to the location of the soil cores. We collected water samples (streams connected to
269 each river) from shallow (< 10-30 cm) permafrost subsidence and hollows with the size of < 1
270 m²; deep depressions (< 1 m) of palsa bogs with sizes ranging from 5 to 15 m²; small thaw
271 ponds with sizes ranging 10-150 m²; and each river closest to the soil core within 5–10 m
272 (depth < 5 m). Neoprene gloves were used during water sampling, and water from the
273 shoreline was collected by a standard PVC MP² two-stop peristaltic pump tubing (1.09 mm
274 I.D., White/Red, Pkg. 12, PerkinElmer, Waltham MA, USA) outfitted with a pre-sterilized
275 Durapore® 0.45 µm capsule filter (MilliporeSigma, Burlington MA, USA). The water
276 passing through the tubing and filter capsules for the first 30 s was not collected, and
277 polypropylene (PPCO) bottles with white PP closure precleaned by 2% nitric acid were used
278 for water collection. The analysis of trace metals in water samples was the same as in
279 subchapter 2.2. The samples used for chloride determination were not acidified. Chloride
280 determination was performed by titration with silver nitrate (AgNO₃, 0.02 mol L⁻¹) as titrant
281 according to ISO 9297: 2000 “Water quality — Determination of chloride — Silver nitrate
282 titration with chromate indicator (Mohr's method).” Titrant calibration was used by
283 standardizing AgNO₃ solution versus NaCl solution with the same molar concentration (0.02

284 mol L⁻¹). The relative standard deviation (RSD) of titrant was <1 %.

285 **3. Results**

286 **3.1 Characteristics of soil profile and chemical composition in the soil column**

287 The detailed horizon and vegetation information in the soil pit profiles in the photographs
288 for SY, MU, and TA is shown in **Figure 1**. The soil group belongs to Histic Gleysols
289 (Stagnic), Histic Gleysols (Turbic), and Turbic Cryosols for SY, MU, and TA, respectively.
290 The top fractions of soil horizons from three soil pits all show a high chroma color, with TA
291 being relatively lighter (**Figure 1B**), and all the lower fractions show strong gleyed
292 conditions, which may indicate a redox boundary. The lower fractions of soils were further
293 tested by a few drops of alpha-alpha-dipyridyl for 30–40 s, showing that no pink color was
294 observed for SY at the depth of 6–9 cm, with a strip-shaped iron oxidized boundary to the
295 next horizon. A positive pink color was observed during the reaction in the next gray color
296 horizon (9-18 cm), suggesting the occurrence of reduced ferrous oxides under the reducing
297 condition. Compared with the previous horizon, this horizon had few plant roots and little
298 accumulation of organic matter. The lowest section (18-35 cm depth) had a sporadic positive
299 pink color. This difference may be due to the different redox spots visually observed in the
300 excavated soil pit (**Figure 1C**). The lower 18–35 cm showed heterogeneous rusty-gray color
301 as the ferric irons, as well as aluminum, and inclusions of organic materials due to the
302 cryogenic mass exchange through bottom-up transportation of water by thawing/freezing
303 processes that bring parent materials to the upper layers, where cracks can be observed in 18–
304 35 cm. In the upper 6–9 cm horizon, the oxidation of ferrous iron to ferric iron is mostly due
305 to the leaching process of upper thawing water containing oxygen. Therefore, the low density
306 of strictly reduced gleyed horizon (6-9 cm) separated the two different geochemical transport
307 pathways between the upper and lower horizons.

308 For soil pit MU, the pink reaction color was observed at the depth of 7–25 cm (the shape
309 shown as B_{g@} horizon in **Figure 1D**), and the middle part of depth 25–60 cm and 60–65 cm

310 depth. In the B_{g@} horizon, there were more dispersed rust-orange spots and stains that
311 followed the path of roots; these ferrous irons were oxidized by the atmosphere through the
312 growth upper vegetation's roots growing. In the 25–60 cm depth, the apparent presence of
313 cryoturbation with a gray-brown color was observed alongside the dark-gray inclusions from
314 the lower permafrost. The oxidized iron in this horizon results from the multi-year
315 freezing/thawing and lower activities of congeliturbation that transport the materials from
316 both the upper and lower layers. The 60–65 cm depth was completely under the reducing
317 condition with loamy soils in gray color.

318 For soil pit TA, the reducing conditions indicated by a positive pink color were observed
319 below 55 cm. TA shows a mixed O and A horizon within 30 cm that has a brownish-gray
320 color and very few roots, which is common under hummocks in Western Siberia. Within the
321 0–55 cm depth, the lateral ring-shaped layers and mud spots can be observed, which were
322 caused by frost heave when a rounded knoll of ice rises during the freezing time. The
323 evidence of cryoturbation can be seen below 55 cm with the dark gray color, and some moss
324 residues are observed in the fragments of cryoturbation clusters.

325 The vertical elemental concentrations in three soil cores measured by EDX are listed in
326 **Table S1 (Supporting information)** and plotted as logarithmic concentrations in soil core
327 depth in **Figure 2**. The other elements not shown in **Figure 2** did not exhibit a regular pattern
328 under reducing conditions within the soil cores. Mn and Co were enriched in the top mineral
329 layer with organic matter accumulation, which likely because of their complexation with
330 natural organic matter. In contrast, Cr, V, Sr, Ca, Mg, Al, Ti, Cd, Mo, Zr, and Sc increased in
331 lower mineral soil horizons in the three soil cores. In particular, for the MU site, Fe, Cr, and V
332 were only higher in the first gleyed horizon with cryoturbation (7-25 cm) and decreased
333 gradually with increased depth. Al, Ti, Cd, and Sc kept increasing until 40 cm (second gleyed
334 horizon) and then decreased gradually or maintained relatively comparable levels in the
335 deeper layers. As, Mo, and Zr decreased until 40 cm and then increased in deeper mineral
336 horizons mixed with frozen material and at the frozen horizon. Zn, Sr, K, Ca, Na, Mg, and Y

337 were higher in all gleyed horizons.

338 For the SY site, three trends were observed: *i*) relatively slight decrease from top to down
339 within the gleyed horizons for As, Cr, V, Mo, Zr, and Se; *ii*) continuous increase in gleyed
340 horizon depth for Sr, K, Ca, Va, Mg, Al, Ti, and Pb; *iii*) only the Cd content increased sharply
341 in the upper gleyed horizon (9–18 cm) and decreased significantly below 18 cm. For the TA
342 site, the maximum concentration was observed in the gleyed horizon for Cr, V, Sr, Ca, Mg,
343 Al, Ti, Cd, Pb, Mo, Zr, Y, and Sc. These elements were apparently enhanced in reducing
344 fractions, concentrations of which, with respect to the upper layers of soil column, can reflect
345 the soils with increased reducing soil conditions. This obvious demarcation between elements
346 with concentrations either increasing in the upper layers of soil column or accumulating in the
347 lower part of soil column correlates to the variation of redox conditions in the soil pit profile
348 as well. The fluctuation of elemental concentrations in the lower soil cores may also be
349 caused by the effect of cryoturbation.

350 The elemental concentrations of soil porewater are listed in **Table S2** and plotted as the
351 function of depth along the cores (not containing supra-permafrost water) in **Figure 3**. The
352 results showed Ca, Mg, and Ti as soluble species that may be available for transporting supra-
353 permafrost water for all three sites because of the increased concentrations in the deeper
354 fraction of the soil core. Additionally, Al in TA site, Mg in MU site, and Fe in SY site may
355 also have the same potential. To some extent, Mn, Ca, Mg, Al, Ti, and Fe all can be soluble
356 species in both upper and deeper fractions of the soil core, indicating both the transport
357 capability from surface flows and supra-permafrost waters to the river.

358 **3.2 Thermal dynamics within soil depth**

359 The temperatures in multiple depths from the installed thermometers are provided in
360 **Figure 4**. In general, the surface (0 cm) soil temperature corresponds to the variation in
361 ambient temperature in this region. The soils at four different depths in TA, MU, and SY were
362 completely frozen by the end of April as our measurements were initiated. In TA, the thawing
363 of frozen soils (temperature rose above 0 °C) occurred on May 30, 2016 at 0 cm, on June 7,

364 2016 at 20 cm, on June 18, 2016 at 40 cm, and on June 30, 2016 at 75 cm. In MU, the
365 thawing occurred on June 2, 2016 at 0 cm, on July 14, 2017 at 25 cm, on June 25, 2016 at 40
366 cm, and on July 4, 2016 on 59 cm. In Sy, the thawing occurred on June 1, 2016 at 0 cm, on
367 June 11, 2016 at 18 cm, on June 22, 2017 at 26 cm, and on July 2, 2016 at 38 cm. The frozen
368 soils in the Arctic notably thaw from top down during the spring-summer season. The lower
369 latitude of TA results in a relatively earlier thawing time than that of MU and SY.

370 **3.3 Chemical composition in the supra-permafrost water**

371 All measured elemental concentrations are plotted as the function of sampling time in
372 **Figure 5** and the pH values for supra-permafrost water in TA, SY, and MU for different
373 sampling months are presented in **Figure S1** with a detailed description in **Text S1**. In TA,
374 the contents of Zn, Mn, Ti, and Sr increased generally from the beginning of summer (June)
375 while Sr and Ti increased slightly with an obvious increasing trend at the end of summer
376 (September 15, 2016). Zn reached its highest concentrations ($15.93\text{-}17.50 \mu\text{g L}^{-1}$) at the
377 beginning of autumn, and this level was maintained until October 2016. Unlike Zn, the peak
378 value of Mn was observed in October. Fe concentrations started to rise significantly at the end
379 of September and peaked at the end of October 2016 ($2049.71 \mu\text{g L}^{-1}$). Mg, Cr, V, Pb, Al, and
380 Ca concentrations exhibited less fluctuation over summer with low concentrations until an
381 increasing trend was observed at the beginning of autumn. Na was the only element that
382 showed a gradual increase in concentration over time till October 15, 2016. For Cd and Mo,
383 there was no particular trend, and their levels were low. SY and MU essentially followed the
384 pattern of TA, while the highest Fe concentration in SY was found at the end of October
385 2016.

386 **3.4 Chemical composition in the surrounding hydrological streams and rivers**

387 We measured the elemental concentrations of the surface water surrounding the soil cores,
388 including the connected hydrological flows (i.e., shallow, depression, and thaw ponds) and
389 rivers (the sites receive the flow), which are shown in **Figure 6**. The pH values for TA, MU,

390 and SY for different months are shown in **Figure S2** with detailed description in **Text S2**. The
391 concentrations of CO₂, CH₄, and DOC in the surrounding streams are plotted as the function
392 of sampling time in **Figure S3** and described in **Text S3**.

393 The remaining detected elements were not shown here because they were below the
394 detection limits. The three sites showed strong similarity of elements' distribution in the
395 connected surface flows and the adjacent rivers with the passage of time. Most elements (i.e.,
396 Fe, Mn, Zn, Na, Pb, Al, and Ca) showed a dramatically increasing trend from the beginning
397 of September to the beginning of October, while Co, V, and Sr significantly increased
398 beginning in August, and only Cr increased starting in July. These elements in the
399 surrounding hydrological streams or rivers reached their highest concentrations at the
400 beginning of October, except for Mo, Cd, and Ti, which had very low concentrations at all
401 time-scales with a slightly increased concentration in October. The concentrations of Fe, Zn,
402 Al, Co, and Sr were consistent with the observation of enhanced soluble concentrations in
403 supra-permafrost water for each of the corresponding months. This may be because of the
404 solubility of these metals, except Co and Mn, which remained at low levels in the top layers
405 of soil cores, and because of the different solubilities of the metals during snow melting,
406 which are related to the bonding mechanism in the soil, especially for top soil layers with
407 increased organic matter. The highest to lowest concentrations for metals were approximately
408 $Fe > Mn > Zn > Sr > Ti > V \approx Na \approx Al \approx Pb > Cd \approx Mo$.

409 **4. Discussion**

410 **4.1 Variability of elemental concentrations in solid soil and soil porewater**

411 In the TA soil column, higher elemental concentrations in soil porewater, such as Mn,
412 Mg, and Ti, were found in the oxidizing zone (~10-15 cm, the layer with organic matter
413 accumulations). Compared with the deeper depth of soil column (~30-83 cm, reducing zone),
414 enhanced elemental accumulations were also observed, especially for Mg and Ti. The lesser

415 extent of Ca and Al concentrations in the top organic layer (**Figure 2**), which may be due to
416 the excess of Ca in the soil solutions, occupy more than 90% of total cation concentration
417 (Leckie 1986). Ca cation can control the soluble stage of trace elements in soils, due to Ca's
418 presentation as an organic complex in soil solutions, preventing the precipitation of soil
419 deposits (Leckie 1986). For instance, fulvic acid in this organic layer can significantly
420 interfere with the crystallization of aluminum hydroxide polymorphs (Kodama and Schnitzer
421 1980). Besides, the aqueous Ti concentrations in both the oxidizing and reducing zones are
422 similar, while Mn is relatively higher in oxidizing zones, and Mg is more enhanced in the
423 reducing zone. Compared with the distribution of these elements in the solid soil core, only
424 Ca and Al showed a similar trend. This difference is due to the soluble and chemical fraction
425 of species.

426 In MU soil column, the concentrations of Mn, Ca, Mg, Al, Fe, and Ti in soil porewater
427 were increased below 7 cm in the reduced zones. However, the solid soil phase shows high
428 levels of Mn in the oxidizing zones (~0-7 cm), with the other elements' distribution
429 corresponding to the soluble forms. In SY soil column, Mn, Mg, and Fe contents in soil
430 porewater were enhanced in the upper oxidizing zones, and Ca content was only obviously
431 enhanced in reduced zones, while Al and Ti both accumulated in the oxidizing and reduced
432 zones. The Mn concentrations were found to be the highest in the oxidizing zones in solid
433 phase, whereas other elements (Ca, Mg, Al, Ti, and Fe) increased in the reduced zones.

434 In both MU and SY, Mn concentrations are found higher in top layer of soil, which is
435 consistent with the low solubility of Mn in lower pH soils (pH = 4.7 for Mu and 4.8 for Sy)
436 (Scholz and Kahlert 2015). We speculate this is because of a more integral gleyed layer (~ 10-
437 40 cm) caused by cryoturbation, which makes the soils share the same origin. SY revealed
438 more heterogenous materials that divided several soil layers through cryoturbation, which
439 results in elemental fluctuations in terms of soluble elements.

440 The three soil cores' depth represents the typical maximum vertical extent during the
441 thawing period in autumn. Among the three soil cores, differences between elemental

442 concentrations in soil porewater and solid soil are still substantial. Taking as an example the
443 concentrations of Mn in the Ta soil column, the concentration of Mn in the oxidizing layer is
444 1039 mg/kg⁻¹ with approximately 0.11 mg/L⁻¹ in soluble form. There is approximately 0.045
445 mg/L⁻¹ mobilized within thawing water to the reduced zones with 388 mg kg⁻¹ presented in
446 solid soil of this layer.

447 To better understand the solubility of elements, the partitioning coefficients (K_d) were
448 calculated as shown in **Figure 7**. Despite the discrepancy of K_d below the top layer, the
449 decreasing solubility can be observed within the gleyed layers, which is consistent with the
450 theory that metals are hindered in this layer (Antcibor et al. 2014). However, Al and Mn were
451 observed with clearly increasing solubility in all soil cores above the permafrost table.
452 Besides, the high partitioning from the solid to the aqueous fraction was observed in Ti for
453 Sy, and Fe and Mn for Mu. Unlike the top organic-rich layers mainly reflecting
454 biogeochemical cycle, minerogenic layers reflect mineralogical weathering. Therefore, the
455 difference may be due to different soil textures and frost processes.

456 The enrichment of Mn and Al for soil materials in Western Siberia was previously
457 investigated (Abakumov et al. 2017, Antcibor et al. 2014, Evgeny et al. 2017, Ji et al. 2019a,
458 Ji et al. 2019b). The further soil water flows into supra-permafrost water, the more it creates
459 consistent input of elements such as Mn and Al from soil to solution. The previous study
460 showed that the solubility of Mn increases with increasing soil acidity (Andrade et al. 2002),
461 which is consistent with our observation. Barker et al. (2014) first reported that trace metals
462 concentrations (Al, Ba, Fe, and Mn) correlate with the seasonal thawed active layer in the
463 Alaskan arctic. This also proves that elemental transport occurred through thawing soil
464 porewater with the potential for those elements to enter surrounding water bodies.

465 **4.2 Elemental fluctuation in supra-permafrost water and surface water by** 466 **seasonal controls**

467 To some extent, except for Mn and Al, some other elements also showed high solubility in

468 the bottom of the three soil cores (**Figure 7**). We expected to see high mobilization of Mn, Al,
469 Ca, and Ti to the supra-permafrost water during spring snow thawing. However, except for
470 Mn, no or very slightly increasing concentrations in the late May / beginning of June can be
471 found in the supra-permafrost water (**Figure 5**), which may be due to the low volume of
472 thawing water or the equilibrium between elemental pool size in solid soils and snowmelt
473 water in the reducing zones at this time. We found the peak concentration time for most
474 elements were shown in late autumn / the beginning of winter. Compared with elements in
475 soil porewater, more elements were above the detection limits and at distinguishable higher
476 levels during the August to October time period. This may indicate that the origin of elements
477 in supra-permafrost water may not only originate from the dilution of snowmelt water within
478 the soil core, while other water flows through the slope of the permafrost table in the
479 landscape. The relatively higher levels of elements such as Mn, Zn, and Fe in TA, than that of
480 SY and MU, could result from the frost heaving of the polygon rim, which released more
481 frozen materials. During summer, thawing starts in the permafrost-affected soils leading to a
482 deeper active layer, which can be shown by the slight increase in Mn, Fe and other elemental
483 concentrations in the supra-permafrost water over the course of June, July, and August. This
484 increase is correlated with the low coefficients in the bottom of the soil core, and with the soil
485 temperature as well. The soil thermal stratification shows that soil temperatures were above 0
486 °C at 0, 20, and 40 cm for TA from late June; in 0, 25, and 40 cm for MU from beginning
487 June; and in 0, 18, and 25 cm for SY from late June whereas the deeper depth (75 cm for TA,
488 59 for MU, and 38 for SY) was still frozen at this time.

489 Most elements revealed relatively high solubility with small K_d values at the deepest depth.
490 In Ta, Mn follows this trend at the depth 18-35 cm, whereas at the deeper depth of 35-40 cm
491 the solubility decreases. The high mobility of these elements in the deeper soil column, along
492 with the latter thawing for these layers, could account for high concentrations in supra-
493 permafrost water and surface water in late September and beginning of October. This pattern
494 is relatively comparable to other elements in TA, MU, and SY, except for Ca and Ti in MU.

495 Generally, elemental fluctuations in the surface flow and river were the same as the supra-
496 permafrost water. The concentrations of Zn, Mn, and Ti in the rivers from July to October
497 were higher than the surface flow, indicating the mobility of these elements to the rivers from
498 the surface flow and include the possibility of contribution to this input from supra-permafrost
499 water. The previous study also showed some metals like Fe, Al, Mn, and Ba decreased in the
500 active layer with subsequent thawing and increasing surface water concentrations during
501 summer to autumn and could indicate elemental transport signals corresponding to the depth
502 dynamics of the active layer (Barker et al. 2014). Our results are consistent with the theory
503 that major and trace elements export to the lakes and rivers through the boundary between the
504 thawed and frozen layers (Raudina et al. 2018). However, we cannot exclude the possibility
505 of abrupt permafrost collapse in the surrounding water body and rivers, which has been
506 shown to enhance metals release into surface water (Loiko et al. 2017). This may also be a
507 reason that not all elements in the surface water were above the detection limits in the soil
508 porewater.

509 **4.3 Potential elemental signatures as a function of organic matter in the surface** 510 **flow**

511 The discharge and source of water are important for the transport of geochemical
512 components such as elements and organic carbon to surface waters. However, it is difficult to
513 determine water sources in cryogenic landscapes with large amounts of ice and multiple
514 flows. In the present study, DOC is used as the “participating media” to estimate elements
515 transported to the surface water; these are considered to be the major carriers of trace
516 elements in boreal and permafrost-affected organic-rich surface waters (Lyvén et al. 2003, Ma
517 et al. 2019, Neubauer et al. 2013, Rember and Trefry 2004, Vasyukova et al. 2010). Due to no
518 pollution from domestic and industrial activities in our sampling sites, the riverine organic
519 carbon is usually subdivided into two origins as the allochthonous pool derived from
520 terrestrial organic matter (topographical erosion and soil leaching) and the autochthonous

521 pool derived from in-situ phytoplankton production (Hope et al. 1994). Additionally, an
522 empirical model for organic carbon exports showed DOC exports to surface runoff is mostly
523 driven by the unfrozen zones during permafrost thawing (Fabre et al. 2019). Therefore, the
524 surface streams with smaller water volume connected between the soils and the rivers were
525 investigated for the relationships between DOC and elements, and the elemental relationship
526 among the streams, rivers, and supra-permafrost waters.

527 The soil in the three study fields all have a top organic layer with sporadic organic
528 distributions in the mineral layers. Previous studies reported that precipitations would form in
529 the rapid surface runoff through supper soil layers with a depth of approximately 15–20 cm
530 (Bishop et al. 1993, Hope et al. 1994). DOC would be exported to the surface water from the
531 top layer without infiltration in the riparian zone. In TA, the highest concentrations of CO₂
532 and CH₄ were observed in the summer snowmelt season with an increasing thawing degree
533 while low concentrations were observed (**Figure 8**), which may have been due to an abrupt
534 thawing process from the top organic layer. This was consistent with the maximal microbial
535 metabolism occurring at the boundary between thawed and frozen permafrost soils in the
536 Western Siberia lowland (Morgalev et al. 2017). However, Dillon and Molot (1997) reported
537 that the release of CO₂ into the boreal waters was increased when the DOC concentration was
538 elevated in the thermokarst lakes. We found a slight decrease in CO₂ and CH₄ when the DOC
539 concentrations reached its peak in Autumn in TA. However, a different pattern was observed
540 in SY and MU in that CO₂ and CH₄ did not increase significantly during snow-ice melting in
541 the spring and summer seasons, while an increasing trend was observed for DOC contents in
542 the surface water. Manasypov et al. (2015) reported no significant enrichment of CO₂ and
543 CH₄ in the thermokarst water bodies during the spring flood through the base flow and further
544 observed that CO₂ levels only increased in small depressions (<10 m²), which is consistent
545 with the ponds (approximately 1 m²) that we sampled. Although some obvious buildup of
546 CO₂ was found in the summer for SY, the results are still comparable to the phenomena in
547 high latitude lakes (Karlsson et al. 2013). The reason for the contrast between TA and the

548 other sites (SY and MU) could be caused by the low volume of the water pond in SY, and in
549 MU due to the low ice contents and a short period suitable for this type of accumulation in
550 low elevations. However, there is also a possibility that more ice existing in polygon rim and
551 buried talik would lead more the more unfrozen water flowing to the surrounding streams.
552 Combination of the results of three sites shows that the response mechanism of enhancing
553 CO₂ in the streams during snow melting is heterotrophic respiration of allochthonous DOM,
554 as approved by the constantly elevated DOC concentrations in this period. However, we
555 suggest the bio-utilization of these carbon types in small ponds may vary according to the
556 contents of materials by different water volumes.

557 The elements with high mobility in the bottom gleyed layer of the soil column and obvious
558 higher concentrations during the snowmelt period were plotted against the DOC (**Figure 8**).
559 In Ta, Mn increased sharply in the summer while Al, Ca, and Mg did not significantly
560 increase. Peak values of Mn, Al, Ca, and Mg with DOC were observed in autumn. The same
561 pattern was observed for SY and MU, especially for Mn. This may indicate the release of
562 micronutrients as Mn during vegetation activity and upper moss litter leaching in the warmer
563 water, which allows higher mobility within the soil column. Because we did not observe a
564 high concentration of Mn in the uppermost soil layer (**Figure 2**), we speculate this
565 contribution of Mn may be from the supra-permafrost water.

566 Another difference found in the TA site was that elemental concentrations (Al, Ca, and
567 Mg) in autumn were significantly higher in comparison to MU and SY, which may be a result
568 of upwelling via the icy cracks beginning as early as October, producing organic- and Fe-
569 accumulated allochthonous ice crystallized at the pond surface. The maximum values of these
570 elements peak during autumn in the surface water are about 2 to 3 times greater than in spring
571 and summer, representing the highest water flow including DOC and dissolved elements.

572 Additionally, the strong linear correlation of Mn between surface streams and rivers was
573 found for all three sites, and that of Al between the surface streams and river was found for Ta
574 (**Figure 9**). However, when comparing the surface streams and supra-permafrost water, Mn

575 was correlated for all three sites; Al only for TA and SY; and Ca only for TA (**Figure 10**).
576 For Mn, the snowmelt flows had higher Mn contents attributed to the increasing mobility of
577 Mn species to other elements in superficial layers of soil as previously reported (Barker et al.
578 2014). Supra-permafrost water also initially contributes to the surface flows and then further
579 flows to the river. The differences for Al and Ca may be due to the different water–soil
580 interactions. Therefore, Mn could be a seasonal signature of autumn representing the
581 dominance of overland surface flow and maximum interactions with the active layer when the
582 active layer is the deepest.

583 **5. Conclusion**

584 This study found that the levels of elements did not begin to increase when the surface
585 temperature is above 0 °C, and the deeper soil column temperature is above 0 °C in late
586 summer/early autumn. The patterns for surrounding water ponds, adjacent river surface
587 waters, and supra-permafrost waters were generally comparable for most elements above
588 detection limits (Zn, Mn, Sr, Fe, Mg, Cr, Co, V, Pb, Al, and Ca) and were highest during the
589 period from September to October, corresponding to the deepest depth of the active layer.
590 Although a geochemical barrier in the reducing gleyed layers was observed in the soil
591 column, some elements (Mn, Ca, Mg, Al, and Ti) still have high mobility above the
592 permafrost table. Additionally, Mn may flow into surrounding water flows (to the river) by
593 both upper soil and supra-permafrost waters transporting organic matter including CH₄ and
594 CO₂. However, heterogenous landscapes with more ice and cryoturbation may cause more
595 elements to move to the surface waters in the present study. Mn in surface flow may be a
596 proxy for the active layer process during the period of summer and autumn. Highly dynamic
597 Arctic hydrological systems that receive geochemical elements from surrounding permafrost
598 soils and delivering more DOC and elements to adjacent hydrological systems. Future climate
599 conditions will intensify the soil–stream–river process due to permafrost degradation and the
600 dynamics of the active layer.

601 Acknowledgements

602 This work was supported by a grant from the Russian Foundation for Basic research (18-
603 44-890003, 16-34-60010 and 19-416-890002); by Jiangsu Nature Science Fund
604 (BK20151378) and the Fundamental Research Funds for the Central Universities
605 (090514380001); by a grant from Saint-Petersburg State University "Urbanized ecosystems of
606 the Russian Arctic: dynamics; state and sustainable development (grant number: 39377455)".
607 We would like to thank Miss Yu Su from the School of Visual Arts at BFA Computer Art for
608 helping with data visualization, and Miss Kuznetsova Ekaterina from School of Journalism
609 and Communication, Tsinghua University for helping with the Russian translation. All data
610 used in figures for analysis are provided in uploaded file "raw data".

611 **References**

- 612 Abakumov, E., Shamilishviliy, G. and Yurtaev, A. (2017) Soil polychemical contamination on
613 Belyi Island as key background and reference plot for Yamal region, p. 313.
- 614 Alekseev, I. and Abakumov, E. (2018) Permafrost-affected former agricultural soils of the
615 Salekhard city (Central part of Yamal region).
- 616 Andrade, E., Miyazawa, M., Pavan, M.A. and Oliveira, E.L.d. (2002) Effect of Organic
617 Matter on Manganese Solubility. *Brazilian Archives of Biology and Technology* 45, 17-20.
- 618 Antcibor, I., Eschenbach, A., Zubrzycki, S., Kutzbach, L., Bolshiyarov, D. and Pfeiffer, E.M.
619 (2014) Trace metal distribution in pristine permafrost-affected soils of the Lena River delta
620 and its hinterland, northern Siberia, Russia. *Biogeosciences* 11(1), 1-15.
- 621 Barker, A.J., Douglas, T.A., Jacobson, A.D., McClelland, J.W., Ilgen, A.G., Khosh, M.S.,
622 Lehn, G.O. and Trainor, T.P. (2014) Late season mobilization of trace metals in two small
623 Alaskan arctic watersheds as a proxy for landscape scale permafrost active layer dynamics.
624 *Chemical Geology* 381, 180-193.
- 625 Bespalaya, Y., Aksenova, O. and Zubriy, N. (2018) Molluscan fauna of the lower reaches of
626 the Syoyakha River (Yamal Peninsula). *Arctic Environmental Research* 18, 76-81.
- 627 Bishop, K.H., Lundström, U.S. and Giesler, R. (1993) Transfer of organic C from forest soils
628 to surface waters: example from northern Sweden. *Applied Geochemistry* 8, 11-15.
- 629 Brown, N.J., Nilsson, J. and Pemberton, P. (2019) Arctic Ocean Freshwater Dynamics:
630 Transient Response to Increasing River Runoff and Precipitation. *Journal of Geophysical*
631 *Research-Oceans* 124(7), 5205-5219.
- 632 Cederstrom, D.J., Johnston, P.M. and Subitzky, S. (1953) Occurrence and development of
633 ground water in permafrost regions.
- 634 Christiansen, H.H., Etzelmüller, B., Isaksen, K., Juliussen, H., Farbrøt, H., Humlum, O.,
635 Johansson, M., Ingeman-Nielsen, T., Kristensen, L., Hjort, J., Holmlund, P., Sannel, A.B.K.,
636 Sigsgaard, C., Åkerman, H.J., Foged, N., Blikra, L.H., Pernosky, M.A. and Ødegård, R.S.
637 (2010) The thermal state of permafrost in the nordic area during the international polar year
638 2007–2009. *Permafrost and Periglacial Processes* 21(2), 156-181.
- 639 Colombo, N., Salerno, F., Martin, M., Malandrino, M., Giardino, M., Serra, E., Godone, D.,
640 Said-Pullicino, D., Fratianni, S., Paro, L., Tartari, G. and Freppaz, M. (2019) Influence of
641 permafrost, rock and ice glaciers on chemistry of high-elevation ponds (NW Italian Alps).
642 *Science of the Total Environment* 685, 886-901.
- 643 Connon, R., Devoie, E., Hayashi, M., Veness, T. and Quinton, W. (2018) The Influence of
644 Shallow Taliks on Permafrost Thaw and Active Layer Dynamics in Subarctic Canada. *Journal*
645 *of Geophysical Research-Earth Surface* 123(2), 281-297.
- 646 Dillon, P.J. and Molot, L.A. (1997) Dissolved organic and inorganic carbon mass balances in
647 central Ontario lakes. *Biogeochemistry* 36(1), 29-42.
- 648 Dvornikov, Y.A., Leibman, M.O., Khomutov, A.V., Kizyakov, A.I., Semenov, P., Bussmann,
649 I., Babkin, E.M., Heim, B., Portnov, A., Babkina, E.A., Streletskaya, I.D., Chetverova, A.A.,
650 Kozachek, A. and Meyer, H. (2019) Gas-emission craters of the Yamal and Gydan peninsulas:

- 651 A proposed mechanism for lake genesis and development of permafrost landscapes.
 652 Permafrost and Periglacial Processes 30(3), 146-162.
- 653 Elder, C.D., Schweiger, M., Lam, B., Crook, E.D., Xu, X., Walker, J., Anthony, K.M.W. and
 654 Czimczik, C.I. (2019) Seasonal Sources of Whole-Lake CH₄ and CO₂ Emissions From
 655 Interior Alaskan Thermokarst Lakes. *Journal of Geophysical Research-Biogeosciences*
 656 124(5), 1209-1229.
- 657 Evgeny, L., Beznosikov, V. and Abakumov, E. (2017) Humic substances elemental
 658 composition of selected taiga and tundra soils from Russian European North-East. *Polish*
 659 *Polar Research* 38, 125-147.
- 660 Fabre, C., Sauvage, S., Tananaev, N., Noël, G.E., Teisserenc, R., Probst, J.L. and Pérez, J.M.S.
 661 (2019) Assessment of sediment and organic carbon exports into the Arctic ocean: The case of
 662 the Yenisei River basin. *Water Research* 158, 118-135.
- 663 Feng, D., Gleason, C.J., Yang, X. and Pavelsky, T.M. (2019) Comparing Discharge Estimates
 664 Made via the BAM Algorithm in High-Order Arctic Rivers Derived Solely From Optical
 665 CubeSat, Landsat, and Sentinel-2 Data. *Water Resources Research*.
- 666 Golovatin, M., Morozova, L.M., Ektova, S.N. and Paskhalny, S.P. (2011) The change of
 667 tundra biota at Yamal Peninsula (the north of the Western Siberia, Russia) in connection with
 668 anthropogenic and climatic shifts. *Tundras: Vegetation, Wildlife and Climate Trends*, 1-46.
- 669 Grosse, G., Goetz, S., McGuire, A.D., Romanovsky, V.E. and Schuur, E.A.G. (2016)
 670 Changing permafrost in a warming world and feedbacks to the Earth system. *Environmental*
 671 *Research Letters* 11(4), 040201.
- 672 Guo, L., Ping, C.-L. and Macdonald, R.W. (2007) Mobilization pathways of organic carbon
 673 from permafrost to arctic rivers in a changing climate. *Geophysical Research Letters* 34(13).
- 674 Hope, D., Billett, M.F. and Cresser, M.S. (1994) A review of the export of carbon in river
 675 water: Fluxes and processes. *Environmental Pollution* 84(3), 301-324.
- 676 Jessen, S., Holmslykke, H.D., Rasmussen, K., Richardt, N. and Holm, P.E. (2014) Hydrology
 677 and pore water chemistry in a permafrost wetland, Ilulissat, Greenland. *Water Resources*
 678 *Research* 50(6), 4760-4774.
- 679 Ji, X., Abakumov, E., Antcibor, I., Tomashunas, V., Knoblauch, C., Zubzycki, S. and Pfeiffer,
 680 E.-M. (2019a) Influence of Anthropogenic Activities on Metals in Arctic Permafrost: A
 681 Characterization of Benchmark Soils on the Yamal and Gydan Peninsulas in Russia. *Archives*
 682 *of Environmental Contamination and Toxicology* 76(4), 540-553.
- 683 Ji, X., Abakumov, E. and Polyakov, V. (2019b) Assessments of pollution status and human
 684 health risk of heavy metals in permafrost-affected soils and lichens: A case-study in Yamal
 685 Peninsula, Russia Arctic AU - Ji, Xiaowen. *Human and Ecological Risk Assessment: An*
 686 *International Journal*, 1-18.
- 687 Johnson, K.D., Harden, J.W., David McGuire, A., Clark, M., Yuan, F. and Finley, A.O. (2013)
 688 Permafrost and organic layer interactions over a climate gradient in a discontinuous
 689 permafrost zone. *Environmental Research Letters* 8(3), 035028.
- 690 Johnston, C.E., Ewing, S.A., Harden, J.W., Varner, R.K., Wickland, K.P., Koch, J.C., Fuller,
 691 C.C., Manies, K. and Jorgenson, M.T. (2014) Effect of permafrost thaw on CO₂ and
 692 CH₄ exchange in a western Alaska peatland chronosequence. *Environmental Research Letters*
 693 9(8), 085004.
- 694 Jorgenson, M.T., Romanovsky, V., Harden, J., Shur, Y., O'Donnell, J., Schuur, E.A.G.,

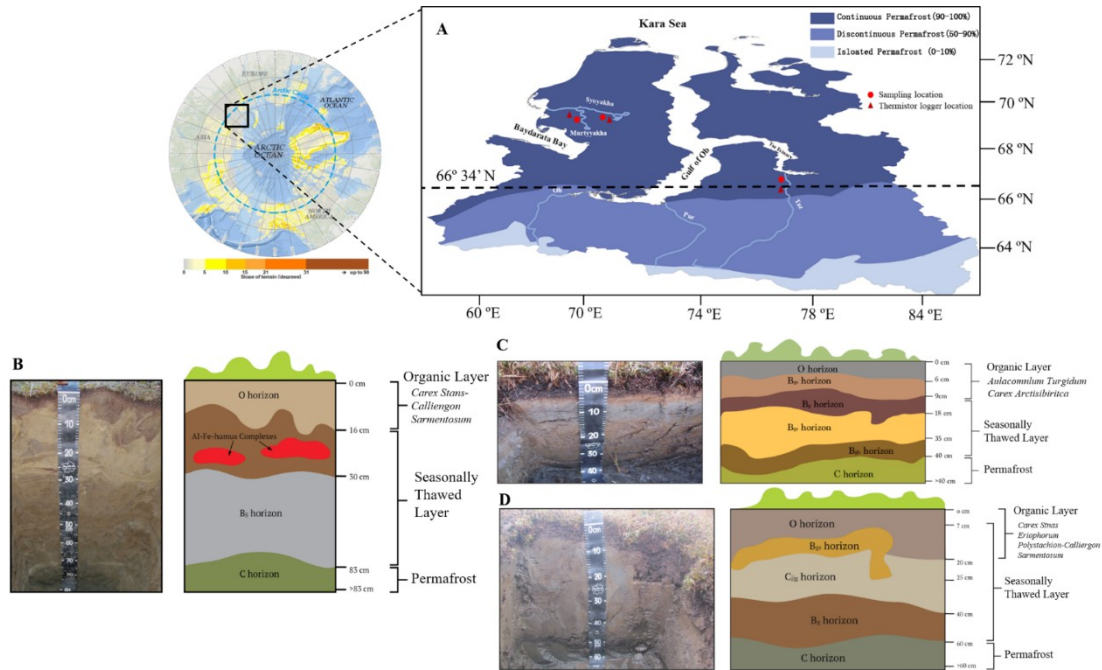
- 695 Kanevskiy, M. and Marchenko, S. (2010) Resilience and vulnerability of permafrost to
696 climate change. *Canadian Journal of Forest Research* 40(7), 1219-1236.
- 697 Karlsson, J., Giesler, R., Persson, J. and Lundin, E. (2013) High emission of carbon dioxide
698 and methane during ice thaw in high latitude lakes. *Geophysical Research Letters* 40(6),
699 1123-1127.
- 700 Kastanidis, P., Michalis, V.K., Romanos, G.E., Stubos, A.K., Economou, I.G. and
701 Tsimpanogiannis, I.N. (2018) Solubility of Methane and Carbon Dioxide in the Aqueous
702 Phase of the Ternary (Methane + Carbon Dioxide + Water) Mixture: Experimental
703 Measurements and Molecular Dynamics Simulations. *Journal of Chemical & Engineering*
704 *Data* 63(4), 1027-1035.
- 705 Keller, K., Blum, J.D. and Kling, G.W. (2007) Geochemistry of Soils and Streams on
706 Surfaces of Varying Ages in Arctic Alaska. *Arctic, Antarctic, and Alpine Research* 39(1), 84-
707 98.
- 708 Keller, K., Blum, J.D. and Kling, G.W. (2010) Stream geochemistry as an indicator of
709 increasing permafrost thaw depth in an arctic watershed. *Chemical Geology* 273(1), 76-81.
- 710 Kodama, H. and Schnitzer, M. (1980) Effect of fulvic acid on the crystallization of aluminum
711 hydroxides. *Geoderma* 24(3), 195-205.
- 712 Lamhonwah, D., Lafrenière, M.J., Lamoureux, S.F. and Wolfe, B.B. (2017) Evaluating the
713 hydrological and hydrochemical responses of a High Arctic catchment during an
714 exceptionally warm summer. *Hydrological Processes* 31(12), 2296-2313.
- 715 Lammers, R.B., Shiklomanov, A.I., Vorosmarty, C.J., Fekete, B.M. and Peterson, B.J. (2001)
716 Assessment of contemporary Arctic river runoff based on observational discharge records.
717 *Journal of Geophysical Research-Atmospheres* 106(D4), 3321-3334.
- 718 Leckie, J.O. (1986) Adsorption and Transformation of Trace Element Species at
719 Sediment/Water Interfaces. Bernhard, M., Brinckman, F.E. and Sadler, P.J. (eds), pp. 237-254,
720 Springer Berlin Heidelberg, Berlin, Heidelberg.
- 721 Liljedahl, A.K., Boike, J., Daanen, R.P., Fedorov, A.N., Frost, G.V., Grosse, G., Hinzman,
722 L.D., Iijma, Y., Jorgenson, J.C., Matveyeva, N., Necsoiu, M., Reynolds, M.K., Romanovsky,
723 V.E., Schulla, J., Tape, K.D., Walker, D.A., Wilson, C.J., Yabuki, H. and Zona, D. (2016) Pan-
724 Arctic ice-wedge degradation in warming permafrost and its influence on tundra hydrology.
725 *Nature Geoscience* 9(4), 312-+.
- 726 Loiko, S.V., Pokrovsky, O.S., Raudina, T.V., Lim, A., Kolesnichenko, L.G., Shirokova, L.S.,
727 Vorobyev, S.N. and Kirpotin, S.N. (2017) Abrupt permafrost collapse enhances organic
728 carbon, CO₂, nutrient and metal release into surface waters. *Chemical Geology* 471, 153-165.
- 729 Lyvén, B., Hassellöv, M., Turner, D.R., Haraldsson, C. and Andersson, K. (2003) Competition
730 between iron- and carbon-based colloidal carriers for trace metals in a freshwater assessed
731 using flow field-flow fractionation coupled to ICPMS. *Geochimica et Cosmochimica Acta*
732 67(20), 3791-3802.
- 733 Ma, Q., Jin, H., Yu, C. and Bense, V.F. (2019) Dissolved organic carbon in permafrost
734 regions: A review. *Science China Earth Sciences* 62(2), 349-364.
- 735 Manasypov, R.M., Vorobyev, S.N., Loiko, S.V., Kritzkov, I.V., Shirokova, L.S., Shevchenko,
736 V.P., Kirpotin, S.N., Kulizhsky, S.P., Kolesnichenko, L.G., Zemtsov, V.A., Sinkinov, V.V. and
737 Pokrovsky, O.S. (2015) Seasonal dynamics of organic carbon and metals in thermokarst lakes
738 from the discontinuous permafrost zone of western Siberia. *Biogeosciences* 12(10), 3009-

- 739 3028.
- 740 McClelland, J.W., Stieglitz, M., Pan, F., Holmes, R.M. and Peterson, B.J. (2007) Recent
741 changes in nitrate and dissolved organic carbon export from the upper Kuparuk River, North
742 Slope, Alaska. *Journal of Geophysical Research: Biogeosciences* 112(G4).
- 743 McCurdy, E. and Woods, G. (2004) The application of collision/reaction cell inductively
744 coupled plasma mass spectrometry to multi-element analysis in variable sample matrices,
745 using He as a non-reactive cell gas. *Journal of Analytical Atomic Spectrometry* 19(5), 607-
746 615.
- 747 Morgalev, Y.N., Lushchaeva, I.V., Morgaleva, T.G., Kolesnichenko, L.G., Loiko, S.V.,
748 Krickov, I.V., Lim, A., Raudina, T.V., Volkova, I.I., Shirokova, L.S., Morgalev, S.Y.,
749 Vorobyev, S.N., Kirpotin, S.N. and Pokrovsky, O.S. (2017) Bacteria primarily metabolize at
750 the active layer/permafrost border in the peat core from a permafrost region in western
751 Siberia. *Polar Biology* 40(8), 1645-1659.
- 752 Natali, S.M., Schuur, E.A.G., Mauritz, M., Schade, J.D., Celis, G., Crummer, K.G., Johnston,
753 C., Krapek, J., Pegoraro, E., Salmon, V.G. and Webb, E.E. (2015) Permafrost thaw and soil
754 moisture driving CO₂ and CH₄ release from upland tundra. *Journal of Geophysical*
755 *Research: Biogeosciences* 120(3), 525-537.
- 756 Neubauer, E., Köhler, S.J., von der Kammer, F., Laudon, H. and Hofmann, T. (2013) Effect of
757 pH and Stream Order on Iron and Arsenic Speciation in Boreal Catchments. *Environmental*
758 *Science & Technology* 47(13), 7120-7128.
- 759 Olefeldt, D. and Roulet, N.T. (2012) Effects of permafrost and hydrology on the composition
760 and transport of dissolved organic carbon in a subarctic peatland complex. *Journal of*
761 *Geophysical Research: Biogeosciences* 117(G1), 页码.
- 762 Ping, C.-L., Clark, M.H., Kimble, J.M., Michaelson, G.J., Shur, Y. and Stiles, C.A. (2013)
763 Sampling Protocols for Permafrost-Affected Soils. *Soil Horizons* 54(1), 页码.
- 764 Ping, C.L., Bockheim, J.G., Kimble, J.M., Michaelson, G.J. and Walker, D.A. (1998)
765 Characteristics of cryogenic soils along a latitudinal transect in Arctic Alaska. *Journal of*
766 *Geophysical Research-Atmospheres* 103(D22), 28917-28928.
- 767 Pokrovsky, O.S., Manasyrov, R.M., Loiko, S.V., Krickov, I.A., Kopysov, S.G.,
768 Kolesnichenko, L.G., Vorobyev, S.N. and Kirpotin, S.N. (2016a) Trace element transport in
769 western Siberian rivers across a permafrost gradient. *Biogeosciences* 13(6), 1877-1900.
- 770 Pokrovsky, O.S., Manasyrov, R.M., Loiko, S.V. and Shirokova, L.S. (2016b) Organic and
771 organo-mineral colloids in discontinuous permafrost zone. *Geochimica et Cosmochimica Acta*
772 188, 1-20.
- 773 Pokrovsky, O.S., Shirokova, L.S., Kirpotin, S.N., Audry, S., Viers, J. and Dupre, B. (2011)
774 Effect of permafrost thawing on organic carbon and trace element colloidal speciation in the
775 thermokarst lakes of western Siberia. *Biogeosciences* 8(3), 565-583.
- 776 Polishchuk, Y.M., Bogdanov, A.N., Muratov, I.N., Polishchuk, V.Y., Lim, A., Manasyrov,
777 R.M., Shirokova, L.S. and Pokrovsky, O.S. (2018) Minor contribution of small thaw ponds to
778 the pools of carbon and methane in the inland waters of the permafrost-affected part of the
779 Western Siberian Lowland. *Environmental Research Letters* 13(4), 页码.
- 780 Raudina, T.V., Loiko, S.V., Lim, A., Manasyrov, R.M., Shirokova, L.S., Istigechev, G.I.,
781 Kuzmina, D.M., Kulizhsky, S.P., Vorobyev, S.N. and Pokrovsky, O.S. (2018) Permafrost thaw
782 and climate warming may decrease the CO₂, carbon, and metal concentration in peat soil

- 783 waters of the Western Siberia Lowland. *Science of the Total Environment* 634, 1004-1023.
- 784 Rember, R.D. and Trefry, J.H. (2004) Increased concentrations of dissolved trace metals and
785 organic carbon during snowmelt in rivers of the alaskan arctic 1 Associate editor: K. F.
786 Falkner. *Geochimica et Cosmochimica Acta* 68(3), 477-489.
- 787 Romanovsky, V.E., Drozdov, D.S., Oberman, N.G., Malkova, G.V., Kholodov, A.L.,
788 Marchenko, S.S., Moskalenko, N.G., Sergeev, D.O., Ukraintseva, N.G., Abramov, A.A.,
789 Gilichinsky, D.A. and Vasiliev, A.A. (2010) Thermal state of permafrost in Russia. *Permafrost
790 and Periglacial Processes* 21(2), 136-155.
- 791 Scholz, F. and Kahlert, H. (2015) The calculation of the solubility of metal hydroxides, oxide-
792 hydroxides, and oxides, and their visualisation in logarithmic diagrams. *ChemTexts* 1(1), 7.
- 793 Schuur, E.A.G., McGuire, A.D., Schädel, C., Grosse, G., Harden, J.W., Hayes, D.J., Hugelius,
794 G., Koven, C.D., Kuhry, P., Lawrence, D.M., Natali, S.M., Olefeldt, D., Romanovsky, V.E.,
795 Schaefer, K., Turetsky, M.R., Treat, C.C. and Vonk, J.E. (2015) Climate change and the
796 permafrost carbon feedback. *Nature* 520, 171.
- 797 Sidorchuk, A. and Grigorev, V. (1998) Soil erosion on the Yamal peninsula (Russian Arctic)
798 due to gas field exploitation , 出版社 , 出版城市.
- 799 Smith, S.L., Romanovsky, V.E., Lewkowicz, A.G., Burn, C.R., Allard, M., Clow, G.D.,
800 Yoshikawa, K. and Throop, J. (2010) Thermal state of permafrost in North America: a
801 contribution to the international polar year. *Permafrost and Periglacial Processes* 21(2), 117-
802 135.
- 803 Street, L.E., Dean, J.F., Billett, M.F., Baxter, R., Dinsmore, K.J., Lessels, J.S., Subke, J.-A.,
804 Tetzlaff, D. and Wookey, P.A. (2016) Redox dynamics in the active layer of an Arctic
805 headwater catchment; examining the potential for transfer of dissolved methane from soils to
806 stream water. *Journal of Geophysical Research: Biogeosciences* 121(11), 2776-2792.
- 807 Tarnocai, C. (2009) Permafrost Soils. Margesin, R. (ed), pp. 3-16, Springer Berlin Heidelberg,
808 Berlin, Heidelberg.
- 809 Vasil'chuk, Y., Budantseva, N., Vasil'chuk, A., Chizhova, J., Podborny, Y. and Vasil'chuk, J.
810 (2016) Holocene multistage massive ice, Sabetayakha river mouth, Yamal Peninsula,
811 northwest Siberia. *GeoResJ* 9-12, 54-66.
- 812 Vasyukova, E.V., Pokrovsky, O.S., Viers, J., Oliva, P., Dupré, B., Martin, F. and Candaudap, F.
813 (2010) Trace elements in organic- and iron-rich surficial fluids of the boreal zone: Assessing
814 colloidal forms via dialysis and ultrafiltration. *Geochimica et Cosmochimica Acta* 74(2), 449-
815 468.
- 816 Walvoord, M.A. and Striegl, R.G. (2007) Increased groundwater to stream discharge from
817 permafrost thawing in the Yukon River basin: Potential impacts on lateral export of carbon
818 and nitrogen. *Geophysical Research Letters* 34(12).
- 819 Wild, B., Andersson, A., Broder, L., Vonk, J., Hugelius, G., McClelland, J.W., Song, W.,
820 Raymond, P.A. and Gustafsson, O. (2019) Rivers across the Siberian Arctic unearth the
821 patterns of carbon release from thawing permafrost. *Proceedings of the National Academy of
822 Sciences of the United States of America* 116(21), 10280-10285.
- 823 WRB (2015) World reference base (WRB) for soil resources, International soil classification
824 system for naming soils and creating legends for soil maps. Food and Agriculture organization
825 of the united nation (FAO), Rome.
- 826 Yang, D.Q., Kane, D.L., Hinzman, L.D., Zhang, X.B., Zhang, T.J. and Ye, H.C. (2002)

827 Siberian Lena River hydrologic regime and recent change. *Journal of Geophysical Research-*
 828 *Atmospheres* 107(D23).

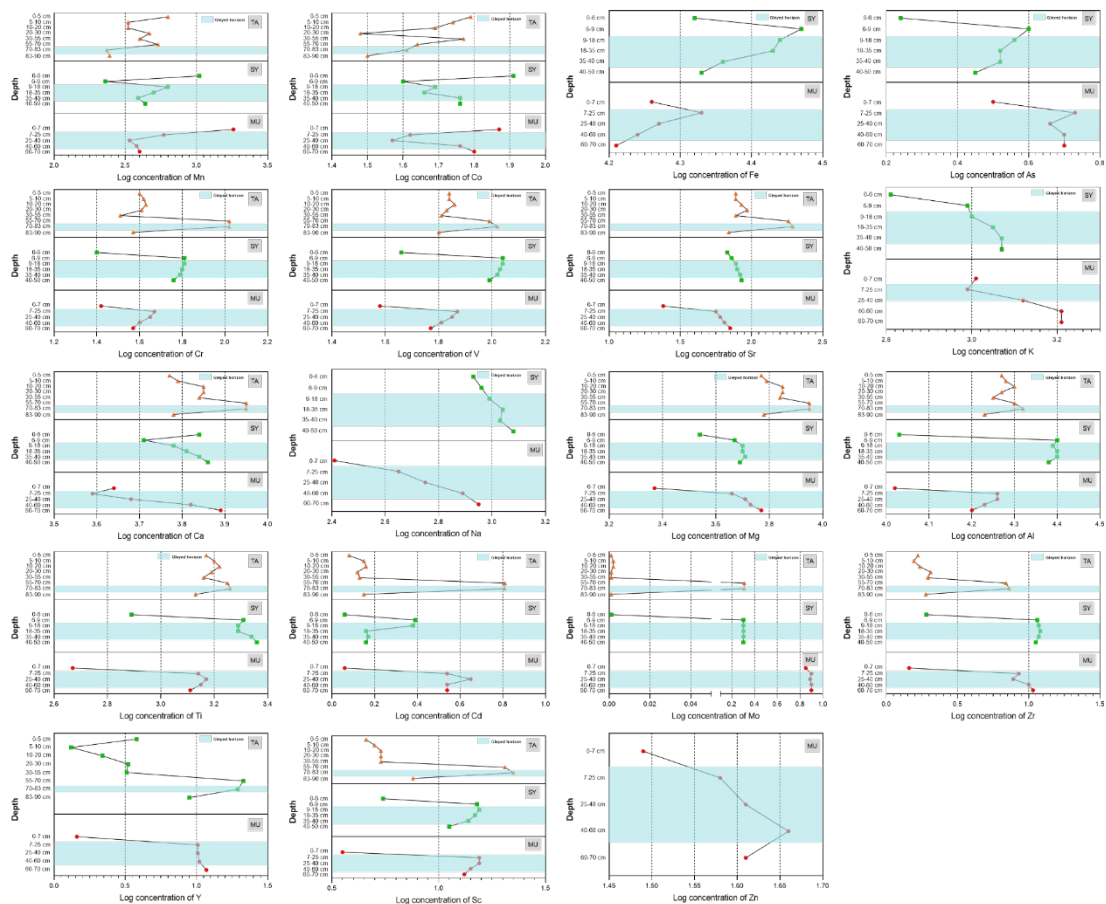
829 Zheng, L., Overeem, I., Wang, K. and Clow, G.D. (2019) Changing Arctic River Dynamics
 830 Cause Localized Permafrost Thaw. *Journal of Geophysical Research-Earth Surface* 124(9),
 831 2324-2344.



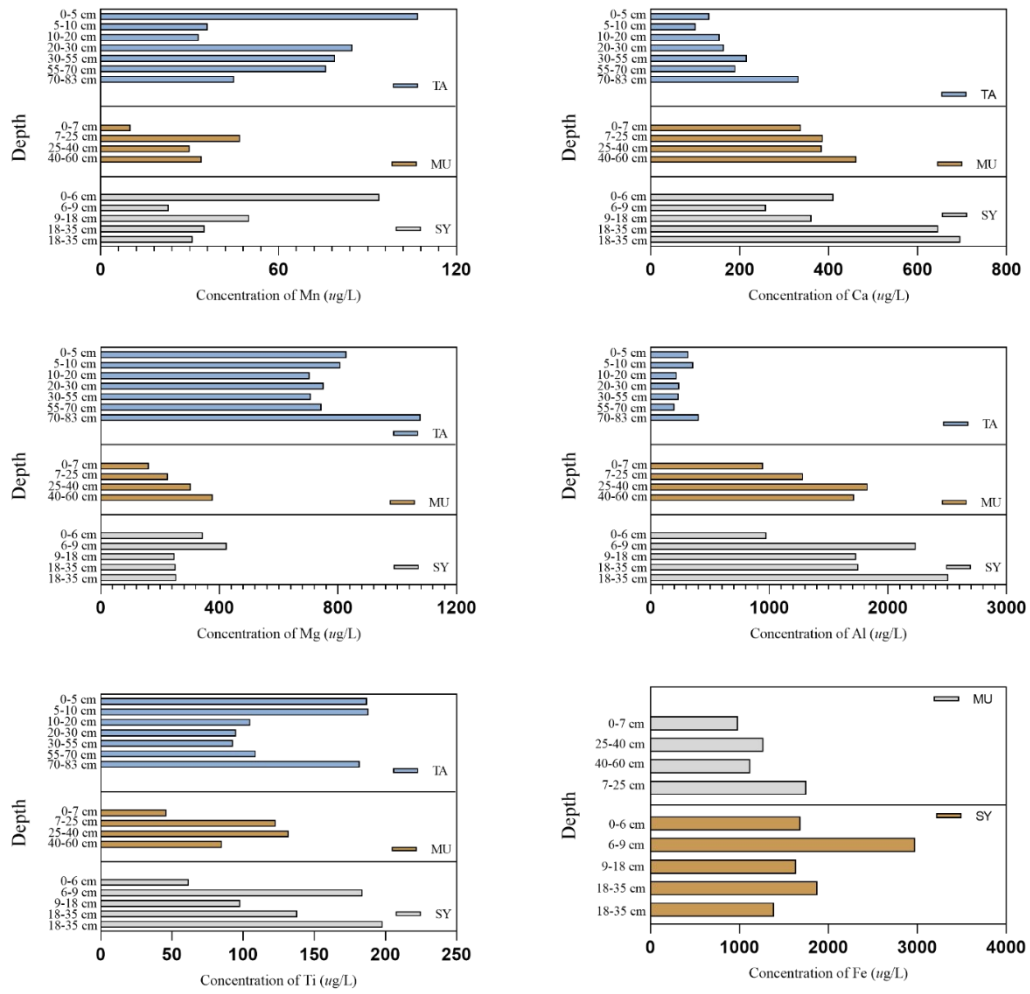
832

833 **Figure 1.** Location of the sampling area and installed thermometer (A). Soil pit profiles and their
 834 upper vegetation species near rivers: (B) Taz river (67°30'13.3"N, 78°40'56.2"E), (C) Syoyakha
 835 river (69°57'03.6"N, 71°23'15.2"E), and (D) Murtyyakha river (70°06'04.7"N, 68°40'24.1"E) in
 836 Yamal-Nets Autonomous Region. All soil profiles are gleyed and have oxidation/reduction
 837 horizons in the upper active layer, substantial top organic layer, and cryoturbation in the lower part
 838 of the active layer.

839

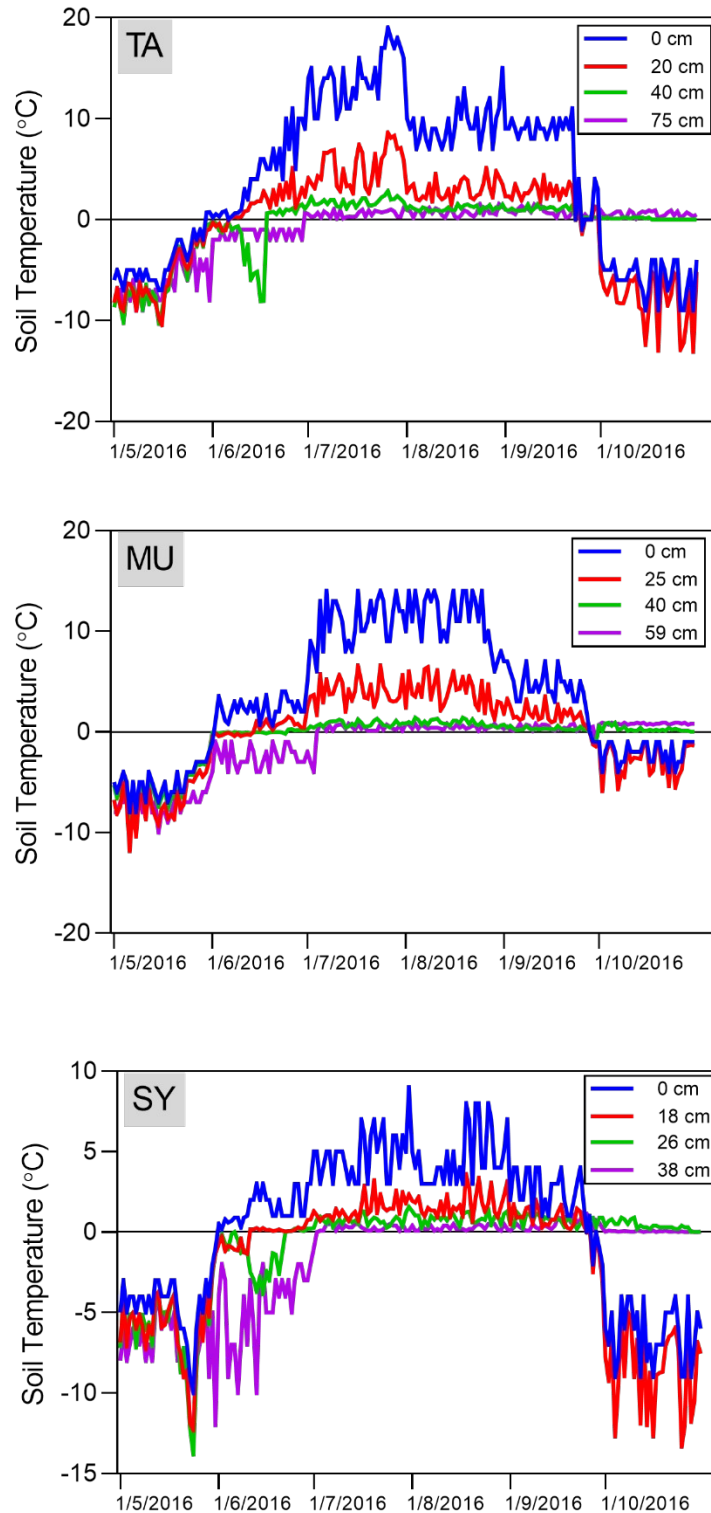


840
 841 **Figure 2.** Vertical metal/element distribution in soil cores collected from TA (Taz river), SY
 842 (Syoyakha river) and MU (Murtyyakha river) sites in the Yamal-Nets Autonomous Region in
 843 beginning May 2016. The logarithmic transformed distribution shows the elements' enrichment
 844 relevant to the top layer with humus accumulation in an oxidizing condition (Mn and Co) and the
 845 lower gleyed layer in a reducing condition.
 846



847

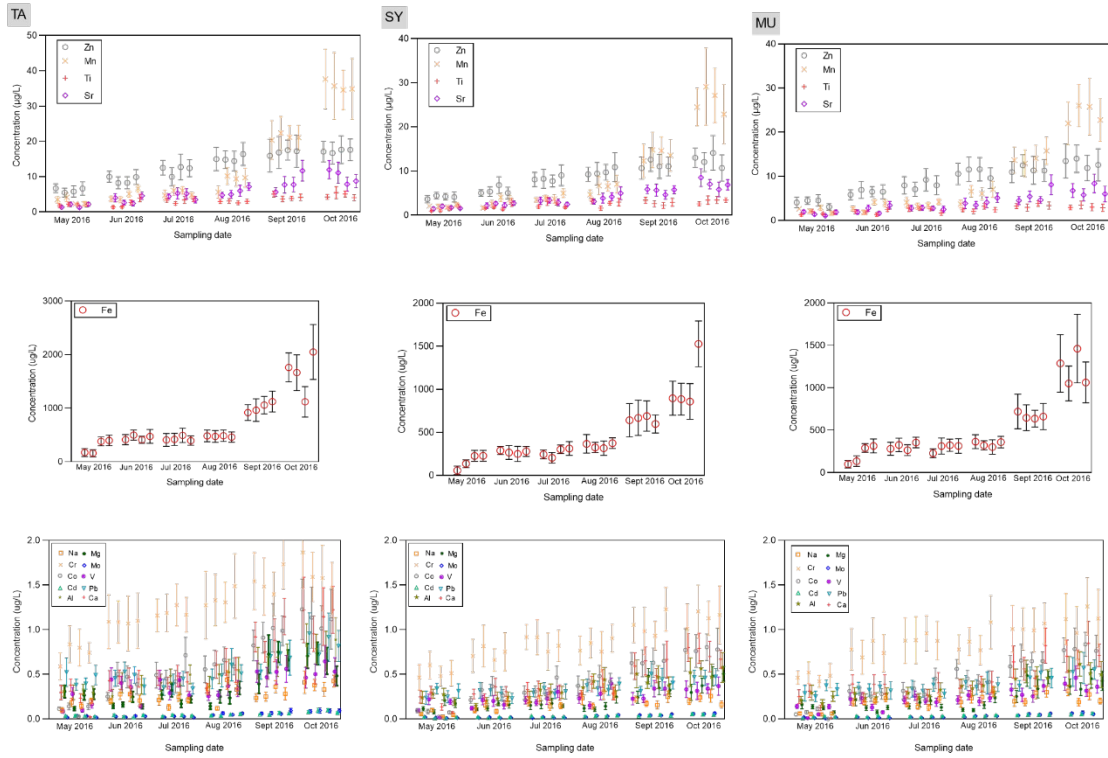
848 **Figure 3.** Distributions of soluble metals along the vertical soil water extracted from the soil
 849 cores collected adjacent to the Ta, Sy, and Mu rivers in the Yamal-Nets Autonomous Region.



850

851 **Figure 4.** Soil temperature (°C) at different soil depths within the active layer as function of
 852 time in 2016. The soil in the Russian Arctic (TA, SY, and MU sites) experiences a top to down
 853 freezing process, making soil porewater flow downwards to deeper soils above frozen
 854 materials (permafrost table).

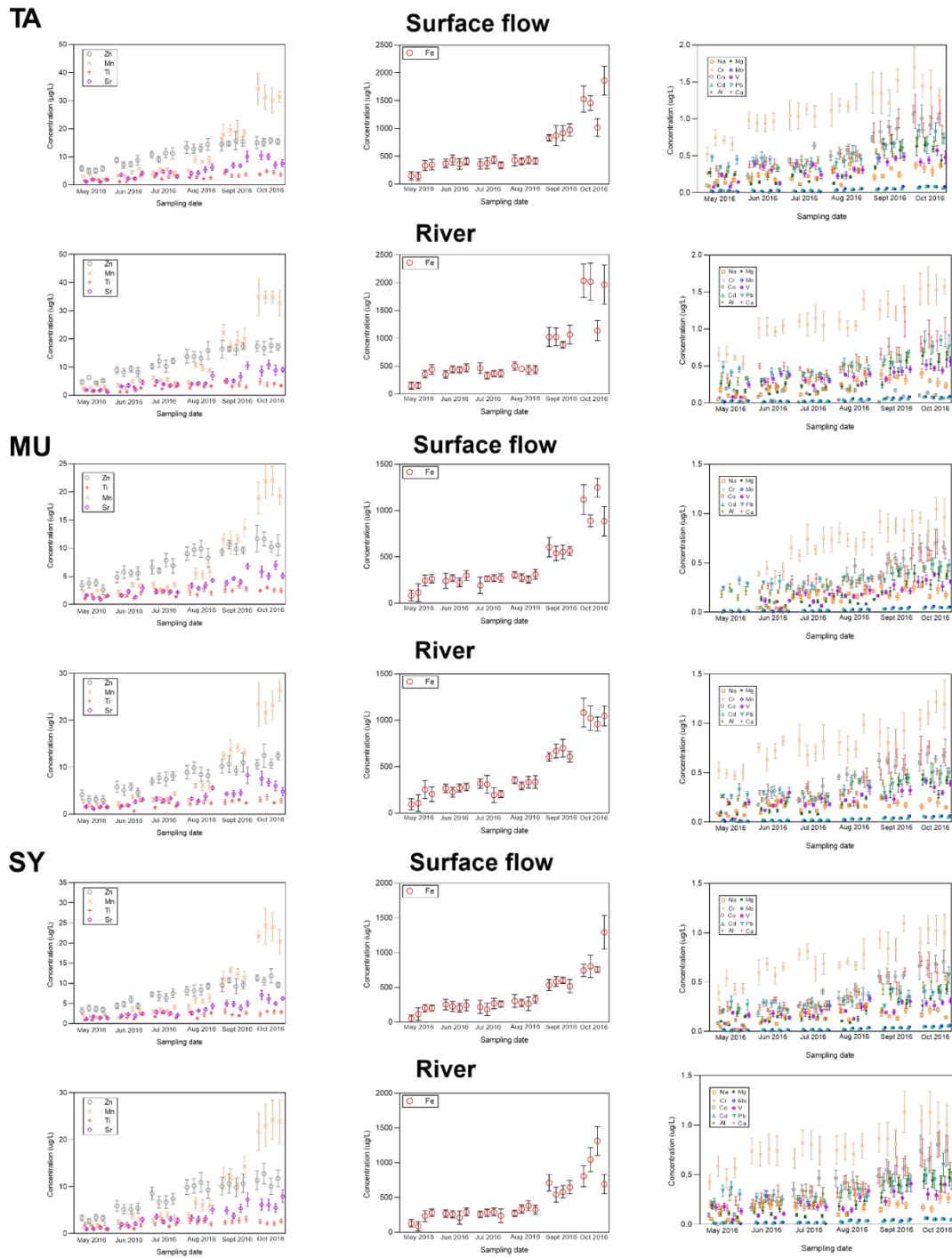
855



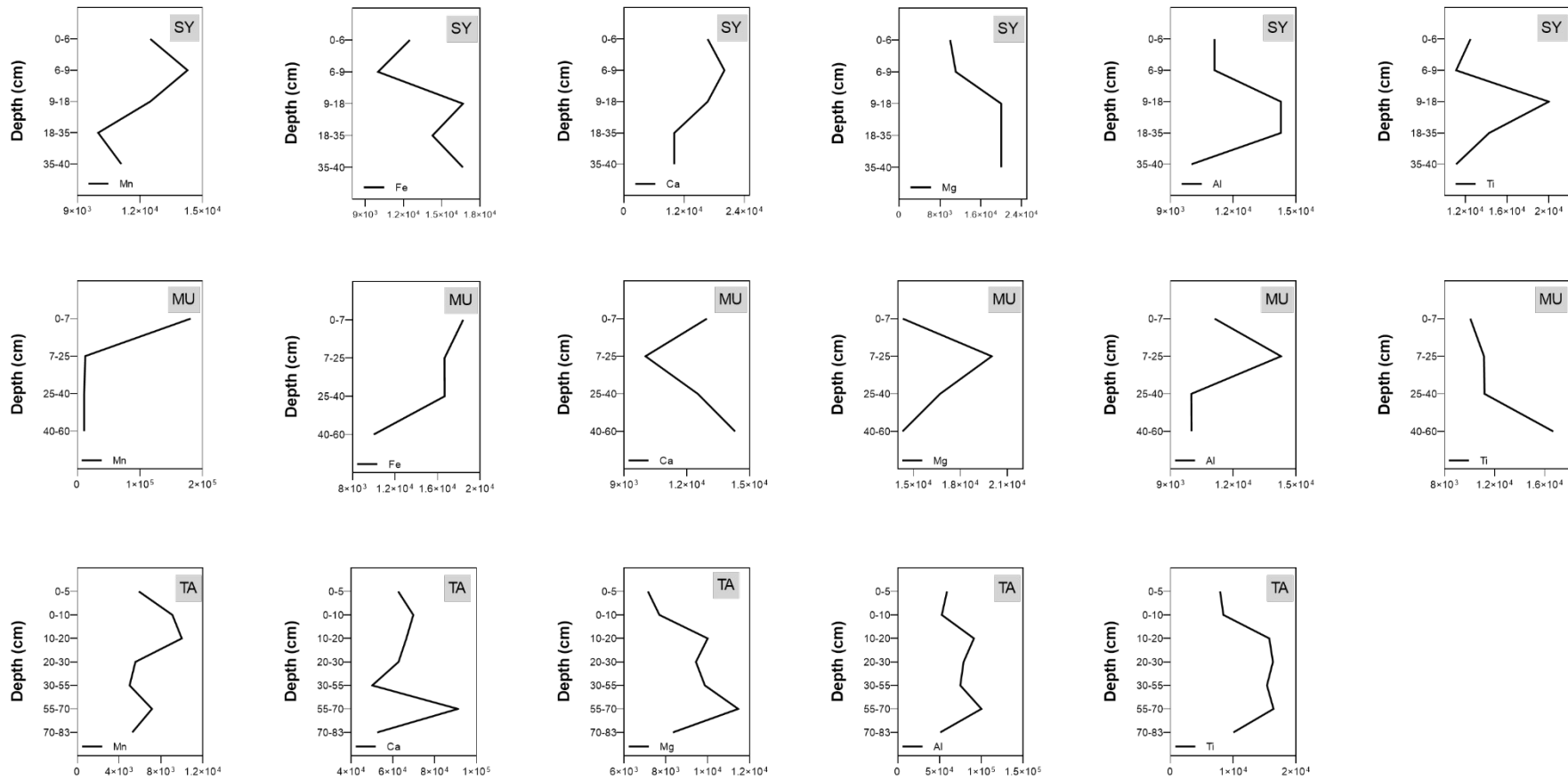
856

857 **Figure 5.** Soluble element concentrations ($\mu\text{g/L}$) in the supra-permafrost water collected from
 858 the Ta, Sy and Mu sites as a function of date in 2016, respectively.

859



860
 861 **Figure 6.** Soluble element concentrations ($\mu\text{g/L}$) in the surface water from connected
 862 hydrological streams to rivers and rivers from the TA, SY, and MU sites as a function of date
 863 in 2016, respectively.



864

865 **Figure 7** Plot of partition coefficients (K_d) for the soil cores from the TA, SY, and MU sites, sampled in the late September 2016
 866 K_d values were calculated by the ratio of elemental concentrations (mg/kg) in the solid soil phase to the elemental

107
 108

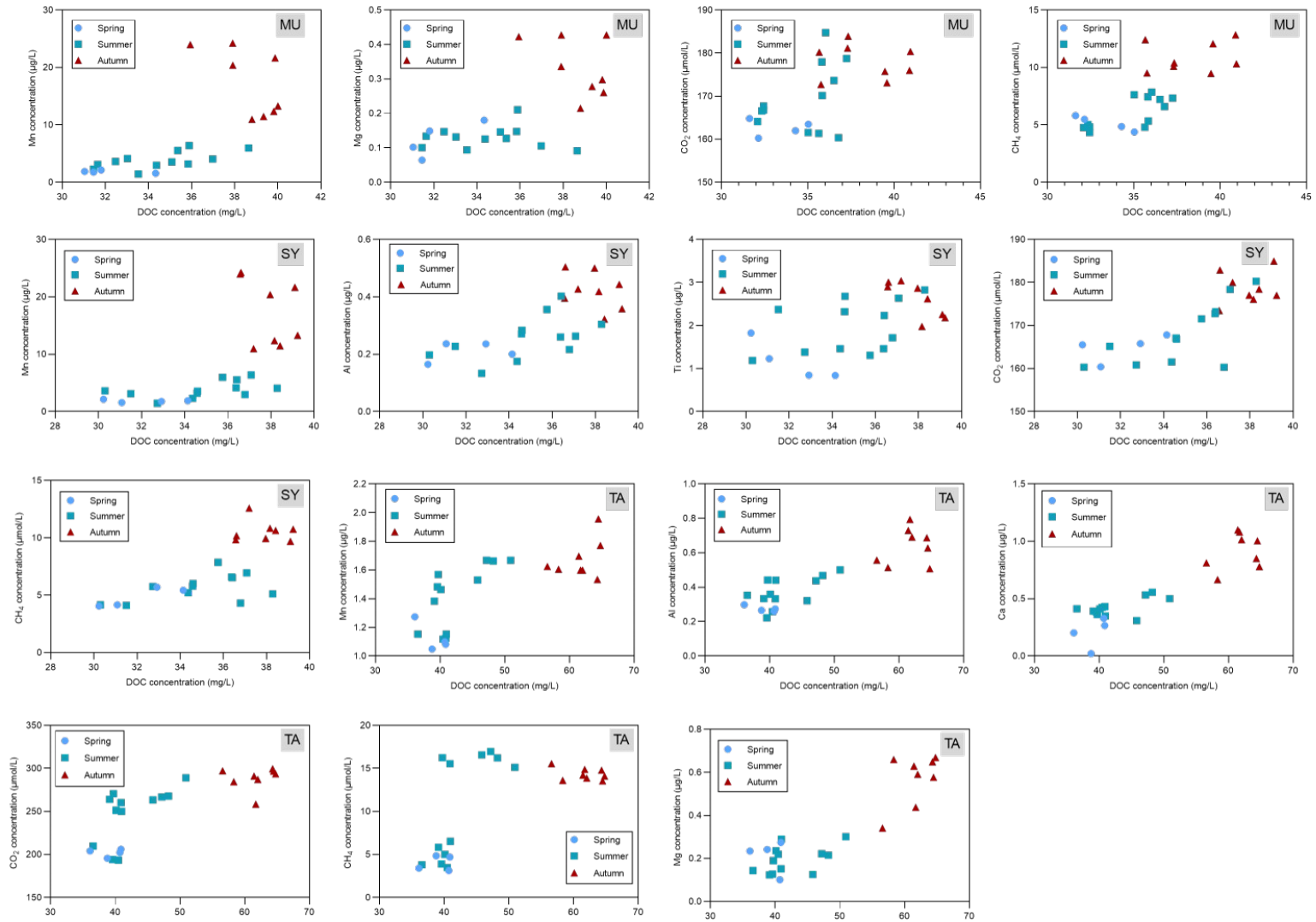
109

867 (m g /

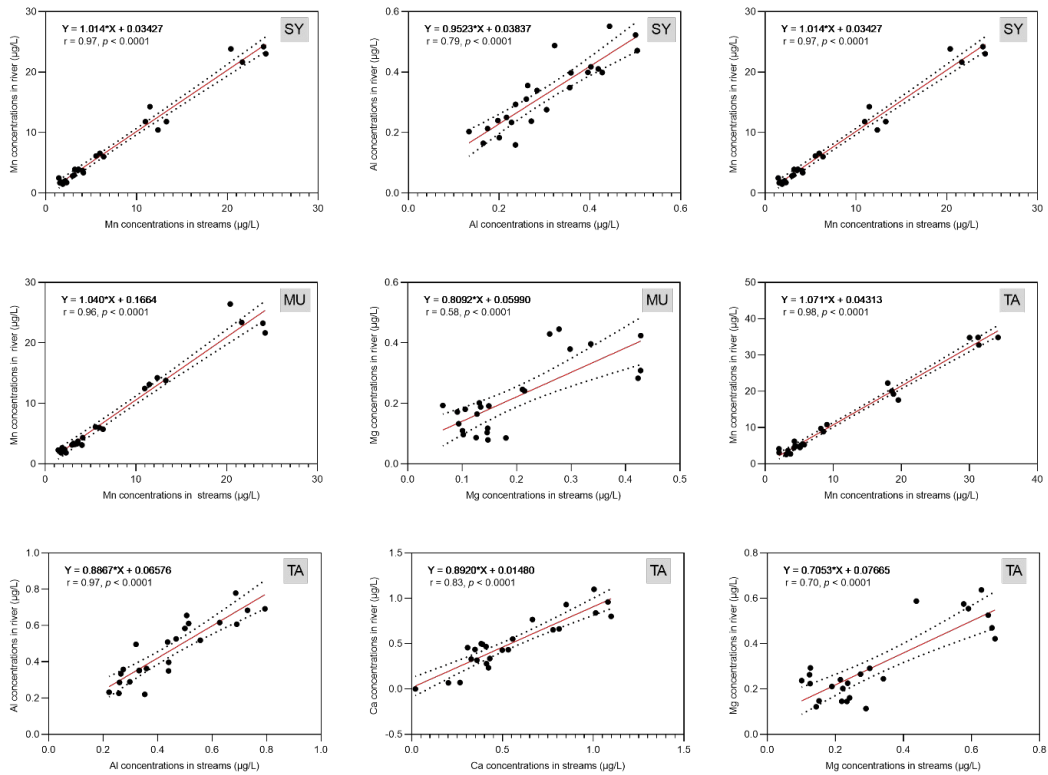
110

111

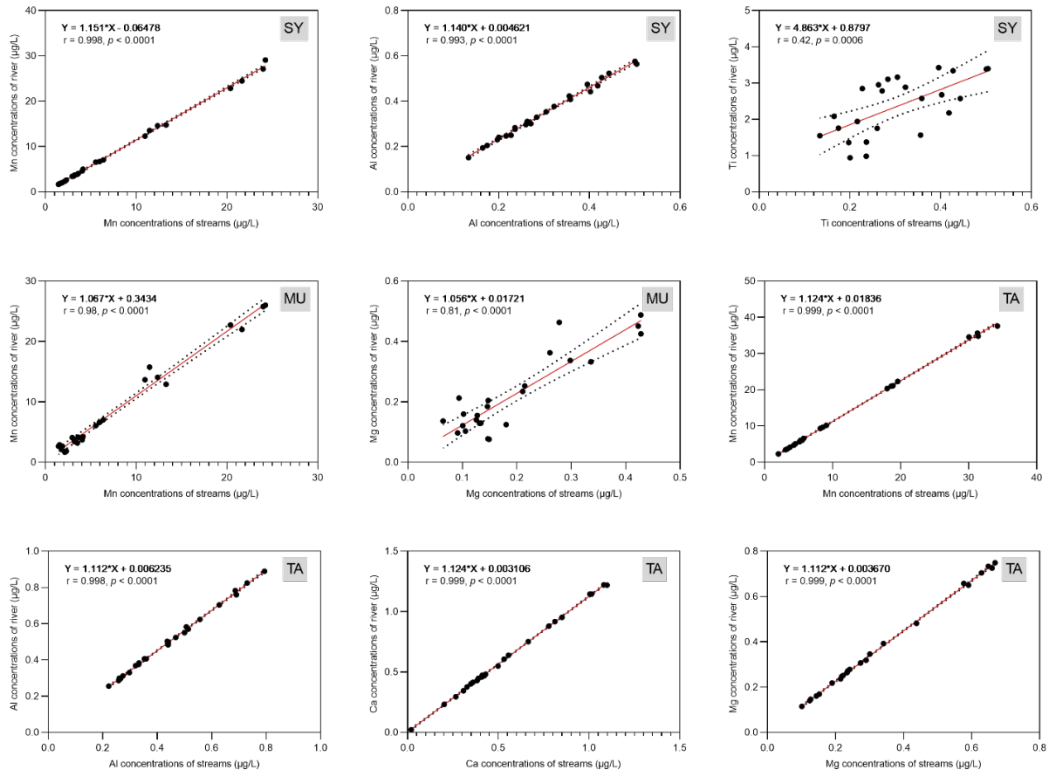
37



870 **Figure 8.** Elements/CO₂/CH₄-dissolved organic carbon (DOC) relationships for the
 871 surrounding hydrological streams in TA, SY, and MU sites over the course of spring to
 872 autumn 2016.



875 **Figure 9.** Linear correlations of the elements with high mobility in soil columns between the
 876 connected surface streams and receiving rivers.



878

879 **Figure 10.** Linear correlations of the elements with high mobility in soil column between the
 880 connected surface streams and supra-permafrost water.